




## RESEARCH ARTICLE

# Propofol inhibits prokaryotic voltage-gated Na<sup>+</sup> channels by promoting activation-coupled inactivation

Elaine Yang<sup>1</sup> , Daniele Granata<sup>2</sup>, Roderic G. Eckenhoﬀ<sup>3</sup>, Vincenzo Carnevale<sup>2</sup> , and Manuel Covarrubias<sup>1</sup> 

Propofol is widely used in the clinic for the induction and maintenance of general anesthesia. As with most general anesthetics, however, our understanding of its mechanism of action remains incomplete. Local and general anesthetics largely inhibit voltage-gated Na<sup>+</sup> channels (Navs) by inducing an apparent stabilization of the inactivated state, associated in some instances with pore block. To determine the biophysical and molecular basis of propofol action in Navs, we investigated NaChBac and NavMs, two prokaryotic Navs with distinct voltage dependencies and gating kinetics, by whole-cell patch clamp electrophysiology in the absence and presence of propofol at clinically relevant concentrations (2–10 μM). In both Navs, propofol induced a hyperpolarizing shift of the pre-pulse inactivation curve without any significant effects on recovery from inactivation at strongly hyperpolarized voltages, demonstrating that propofol does not stabilize the inactivated state. Moreover, there was no evidence of fast or slow pore block by propofol in a non-inactivating NaChBac mutant (T220A). Propofol also induced hyperpolarizing shifts of the conductance-voltage relationships with negligible effects on the time constants of deactivation at hyperpolarized voltages, indicating that propofol does not stabilize the open state. Instead, propofol decreases the time constants of macroscopic activation and inactivation. Adopting a kinetic scheme of Nav gating that assumes preferential closed-state recovery from inactivation, a 1.7-fold acceleration of the rate constant of activation and a 1.4-fold acceleration of the rate constant of inactivation were sufficient to reproduce experimental observations with computer simulations. In addition, molecular dynamics simulations and molecular docking suggest that propofol binding involves interactions with gating machinery in the S4–S5 linker and external pore regions. Our findings show that propofol is primarily a positive gating modulator of prokaryotic Navs, which ultimately inhibits the channels by promoting activation-coupled inactivation.

## Introduction

General anesthetics are used on millions of patients each year and yet remain some of the most toxic and poorly understood drugs, as the exact mechanisms by which they elicit clinical endpoints and adverse effects are not known. Propofol is one of the most commonly used intravenous agents for induction of anesthesia and is often used for maintenance in certain surgical procedures (James and Glen, 1980; Feng et al., 2017). Studies have shown that propofol potentiates some eukaryotic and prokaryotic inhibitory ligand-gated ion channels and inhibits excitatory ones (Hales and Lambert, 1991; Lin et al., 1992; Belelli et al., 1999; Dilger, 2002; Weng et al., 2010; Zhou et al., 2012). Moreover, high-resolution structural studies and photoaffinity labeling experiments have revealed the sites of propofol action in several ligand-gated

ion channels, including GABA<sub>A</sub> receptors and GLIC (Nury et al., 2011; Chiara et al., 2014; Jayakar et al., 2014; Woll et al., 2018). The anesthetic effects of propofol are thus likely due in part to effects on ionotropic receptors. Current models of general anesthetic action, however, suggest that the modulation of multiple protein targets, including other ion channels, is responsible for the clinical endpoints of anesthesia as well as off-target effects (Hemmings et al., 2005; Franks, 2008).

Previous work with isolated rat neurohypophyseal nerve terminals demonstrated that propofol and the inhaled anesthetic isoflurane depress excitatory neurotransmission by inhibiting presynaptic voltage-gated Na<sup>+</sup> channels (Navs; Ouyang et al., 2003). In the nerve terminals, inhibition results from the anes-

<sup>1</sup>Vickie and Jack Farber Institute for Neuroscience and Department of Neuroscience, Sidney Kimmel Medical College and Jefferson College of Biomedical Sciences, Thomas Jefferson University, Philadelphia, PA; <sup>2</sup>Institute for Computational Molecular Science, College of Science and Technology, Temple University, Philadelphia, PA; <sup>3</sup>Department of Anesthesiology and Critical Care, Perelman School of Medicine, University of Pennsylvania, Philadelphia, PA.

Correspondence to Manuel Covarrubias: [manuel.covarrubias@jefferson.edu](mailto:manuel.covarrubias@jefferson.edu); Elaine Yang: [elaine.yang@jefferson.edu](mailto:elaine.yang@jefferson.edu).

© 2018 Yang et al. This article is distributed under the terms of an Attribution–Noncommercial–Share Alike–No Mirror Sites license for the first six months after the publication date (see <http://www.rupress.org/terms/>). After six months it is available under a Creative Commons License (Attribution–Noncommercial–Share Alike 4.0 International license, as described at <https://creativecommons.org/licenses/by-nc-sa/4.0/>).

thetic-induced hyperpolarization of voltage-dependent inactivation, a universal feature of general anesthetics in prokaryotic and eukaryotic Navs (Rehberg and Duch, 1999; Ouyang et al., 2009; Barber et al., 2014; Covarrubias et al., 2015; Sand et al., 2017). Intriguingly, pore-blocking local anesthetics, such as lidocaine and benzocaine, also induce this hyperpolarizing shift (Strichartz, 1973; Hille, 1977; Lee et al., 2012a). According to the modulated receptor hypothesis, local anesthetics bind in the pore of inactivated Navs with high affinity and stabilize the inactivated state, which slows recovery from inactivation and, consequently, hyperpolarizes the voltage dependence of inactivation (Hille, 1977). It is not known, however, whether propofol also inhibits Navs by this mechanism.

To gain biophysical and structural insight into the modulation of Navs by propofol, we investigated NaChBac, from *Bacillus halodurans* (Ren et al., 2001), and NavMs, from *Magnetococcus marinus* (McCusker et al., 2012), two prokaryotic Navs with distinct kinetics and voltage-dependent properties. Despite some differences, prokaryotic Navs exhibit many structural and functional features of their eukaryotic counterparts and have served as excellent surrogates for investigations into ion channel selectivity and conductance, gating, and pharmacology (Nurani et al., 2008; Payandeh et al., 2011; McCusker et al., 2012; Zhang et al., 2012; Ulmschneider et al., 2013; Finol-Urdaneta et al., 2014; Catterall, 2015; Ahern et al., 2016; Naylor et al., 2016). In contrast to the single polypeptide eukaryotic channels consisting of four contiguous, homologous pore-forming domains, prokaryotic Navs are a tetrameric assembly of identical subunits, which is experimentally advantageous for mutational studies. Furthermore, although prokaryotic Navs lack the intracellular inactivation domain responsible for the fast hinged lid mechanism of inactivation, they do exhibit slow inactivation (Catterall, 2001; Pavlov et al., 2005). This has given us the opportunity to ask fundamental questions about the modulation of slow inactivation by propofol, which may underlie the universal hyperpolarizing effect of general anesthetics on steady-state inactivation in Navs.

Several published studies have used prokaryotic Navs to investigate mechanisms of local and general anesthetic action. Biophysical studies suggest that local anesthetics block NaChBac and NavMs and promote entry into the inactivated state (Lee et al., 2012a), and crystallographic studies have linked these functional effects to drug binding sites within the pore domain (Bagn  ris et al., 2014). Volatile general anesthetics such as isoflurane and sevoflurane promote activation and inactivation gating in NaChBac (Ouyang et al., 2007; Barber et al., 2014; Sand et al., 2017), but open pore block has not been ruled out. Molecular dynamics (MD) simulations and <sup>19</sup>F-NMR studies have proposed novel volatile anesthetic binding sites, including a subset in the pore domain that may overlap with local anesthetic binding sites (Raju et al., 2013; Barber et al., 2014; Kinde et al., 2016). The binding sites associated with the mechanism of action of propofol in Navs, however, have not been explored.

Our results demonstrate that propofol modulates NaChBac and NavMs in a similar fashion, despite differences in their kinetics and voltage-dependent properties. Results from NavMs are particularly significant in that its modulation by general anesthetics has not previously been reported and that its full-length

crystal structure was recently solved (Sula et al., 2017), allowing structural interpretation of biophysical results and direct modeling of potential interactions. Here, we show that propofol primarily accelerates voltage-dependent activation and separately accelerates slow inactivation to a more modest degree. Recovery from inactivation and deactivation are largely unaffected, and furthermore, there is no evidence of open pore block. The modulated receptor mechanism of local anesthetics thus fails to describe the mechanism of action of propofol on these Navs. Instead, propofol inhibits these Navs by promoting activation and, subsequently, activation-coupled slow inactivation. Consistent with the functional results, MD simulations of NavMs revealed two potential propofol binding sites: an extracellular pocket near the selectivity filter at the intersubunit interface and an intracellular pocket lined by the S4–S5 linker and S6 helix of neighboring subunits. To link functional effects with structural elements of the ion channels, the companion article by Wang et al. in this issue uses <sup>19</sup>F-NMR to probe putative propofol binding sites in NaChBac. Altogether, this study elucidates the biophysical and molecular basis of propofol action on prokaryotic Navs and provides a sound starting point for future investigation of the mechanisms of propofol action on eukaryotic Navs.

## Materials and methods

### Molecular and cell biology

WT NaChBac cDNA in a modified pTracer-CMV2 expression vector was a gift from D. Ren (University of Pennsylvania, Philadelphia, PA), and WT NavMs cDNA in a modified pTracer-CMV2 expression vector was a gift from P. DeCaen (Northwestern University, Evanston, IL) and D. Clapham (Harvard University, Boston, MA). cDNA was amplified in bacterial culture and purified with the QIAGEN Plasmid Midi kit. To generate NaChBac T220A, a point mutation was introduced into the WT plasmid using the QuikChange site-directed mutagenesis method (Agilent).

HEK-293 (NaChBac) or HEK-293T (NavMs) cells were transiently transfected with cDNA using the Lipofectamine 2000 transfection reagent (Invitrogen) and seeded onto 12-mm circular glass coverslips 24 h before patch clamp recording. Standard protocols were followed for growth and maintenance of cells in culture.

### Electrophysiology

Patch pipettes were pulled from borosilicate capillary glass (LA16; Dagan) with a HEKA PIP6 micropipette puller. Before recording, patch pipettes were fire polished to a final resistance of 1.5–2.3 MΩ. Whole-cell patch clamp recording was performed using an Axopatch 200B amplifier (Molecular Devices) and Digidata 1440A analogue-to-digital converter (Molecular Devices). Series resistance was compensated at least 85%. Passive leak current and capacitive transients were subtracted online by standard P/4 protocol (NaChBac) or offline using the passive leak subtraction feature in pCLAMP (NavMs). All recordings were low-pass Bessel-filtered at 2 kHz and digitized at 15.4 kHz. Clampex 10 (pCLAMP 10; Molecular Devices) was used to control voltage protocols and for data acquisition.

For NaChBac recordings, the extracellular bath solution contained (in mM) 140 NaCl, 4 KCl, 1.5 CaCl<sub>2</sub>, 1.5 MgCl<sub>2</sub>, 10 HEPES, and 5 D-glucose, pH 7.3, adjusted with NaOH; the intracellular pipette solution contained (in mM) 15 NaCl, 80 CsF, 40 CsCl, 10 EGTA, and 10 HEPES, pH 7.3, adjusted with CsOH. For NavMs recordings, the extracellular bath solution contained (in mM) 150 NaCl, 1.8 CaCl<sub>2</sub>, 1 MgCl<sub>2</sub>, and 10 HEPES, pH 7.4, adjusted with NaOH; the intracellular pipette solution contained (in mM) 30 NaCl, 110 CsF, 1 KCl, 10 HEPES, and 5 EGTA, pH 7.4, adjusted with CsOH. Propofol stock solution (400  $\mu$ M in bath solution) was prepared by diluting 2,6-diisopropylphenol (Sigma-Aldrich) in bath solution, followed by alternating sonication and vortexing for 4.5 min. The stock solution was then diluted to working concentrations; all dilutions were prepared and used the same day. Cells were continuously perfused with bath solution at room temperature (22–25°C) during recordings. In all experiments, all control recordings were collected first, before any anesthetic exposure. After control recordings, propofol was perfused for ~3 min before collecting paired anesthetic recordings and continuously thereafter. To prevent inaccuracies caused by any membrane lipid retention of anesthetic molecules and cumulative effects, each experimental cell was only exposed to one concentration of anesthetic, and washout data were not used.

### Voltage protocols

In NaChBac WT and T220A, voltage-dependent activation was assessed with Na<sup>+</sup> currents evoked by 500-ms depolarizing steps (–100 to +60 mV,  $\Delta V$  = 10 mV) from a holding potential of –120 mV. Pre-pulse inactivation was assessed with a two-pulse protocol: (1) a 2-s conditioning pulse (–120 mV to –10 mV,  $\Delta V$  = 10 mV), followed immediately by (2) a 50-ms test pulse to +10 mV. The holding potential was –120 mV. A two-pulse protocol was also used to characterize recovery from inactivation: (1) a 2-s conditioning pulse at –10 mV, followed by (2) a 50-ms test pulse to –10 mV. The pulses were separated by a variable recovery interval ( $\Delta t$  = 10 ms to 12 s) at –120 mV. The rate of inactivation at –55 mV was determined with a two-pulse protocol: (1) a conditioning pulse of variable duration ( $\Delta t$  = 10 ms to 5 s) at –55 mV, followed by (2) a 50-ms test pulse to –10 mV. The holding potential was –140 mV. Deactivation currents were elicited by 900-ms hyperpolarizing steps (–120 to –60 mV,  $\Delta V$  = 10 mV) after a short 15–20 ms activating pulse to –10 mV.

In NavMs, voltage-dependent activation was assessed with Na<sup>+</sup> currents evoked by 200-ms depolarizing steps (–140 to +40 mV,  $\Delta V$  = 10 mV) from a holding potential of –180 mV. Pre-pulse inactivation was assessed with a two-pulse protocol: (1) a 1-s conditioning pulse (–170 mV to –60 mV,  $\Delta V$  = 10 mV), followed immediately by (2) a 50-ms test pulse to –30 mV. Recovery from inactivation was also characterized with a two-pulse protocol: (1) a 500-ms conditioning pulse at –30 mV, followed by (2) a 50-ms test pulse to –30 mV. The pulses were separated by a variable recovery interval ( $\Delta t$  = 10 ms to 10 s) at –180 mV.

### Data analysis

Clampfit 10 (pCLAMP 10, Molecular Devices), Origin 9.1 (Origin-Lab), and Excel 2013 (Microsoft) were used to analyze voltage-clamp data. All evaluated parameters are reported as mean

$\pm$  SEM. The paired samples *t* test was used to assess differences between paired datasets in the absence and presence of propofol. *P* values less than 0.05 are explicitly reported in the figures and figure legends, and NS indicates *P*  $\geq$  0.05.

Peak chord conductance (*G*) was calculated using  $G = I / [V - V_{\text{rev}}]$ , where *I* is the measured peak current, *V* is the command potential, and *V*<sub>rev</sub> is the reversal potential extrapolated from individual current–voltage curves. The voltage dependence of activation (*G*–*V* curve) was derived from the best-fit fourth order Boltzmann function  $G(V) = [G_{\text{max}} / (1 + e^{(V_s - V)/k})]^4$  and normalized to *G*<sub>max</sub>, where *G*<sub>max</sub> is the maximum peak conductance, *V*<sub>s</sub> is the midpoint of activation for a single subunit, *V* is the command potential, and *k* is the slope factor. The midpoint voltage of activation was calculated using  $V_{1/2} = (V_s + 1.67k)$ , and the effective gating charge (*z*) was calculated using  $z = 25.5/k$ . Pre-pulse inactivation parameters were determined from the best-fit first order Boltzmann function  $I(V) = I_{\text{max}} / (1 + e^{(V_{1/2} - V)/k})$  and normalized to *I*<sub>max</sub>, where *I*<sub>max</sub> is the maximum current amplitude and *V*<sub>1/2</sub> is the midpoint voltage of inactivation. Time constants of activation and inactivation were derived from the rising and decaying components of the Na<sup>+</sup> current, respectively, using the best-fit single exponential of the form  $I(t) = (A e^{-t/\tau} + C)$ , where *A* is the amplitude, *C* is the plateau constant, *t* is time, and  $\tau$  is the time constant of activation or inactivation. Time constants of deactivation were derived from tail current relaxations using the best-fit double exponential of the form  $I(t) = (A_1 e^{-t/\tau_1} + A_2 e^{-t/\tau_2} + C)$  as a weighted mean of  $\tau_1$  and  $\tau_2$ , where *A*<sub>*n*</sub> is the *n*<sup>th</sup> component amplitude and  $\tau_n$  is the *n*<sup>th</sup> component time constant. Time courses of recovery from inactivation were determined by plotting fractional recovery from inactivation ( $I_{\text{peak, pulse 2}} / I_{\text{peak, pulse 1}}$ ) against the recovery interval ( $\Delta t$ ). Time constants of recovery were then derived from the time courses of recovery using the best-fit single exponential of the form  $y(t) = [y_0 + A (1 - e^{-t/\tau})]$ , where *A* is the amplitude,  $\tau$  is the recovery interval,  $\tau$  is the time constant of recovery from inactivation, and *y*<sub>0</sub> is the *y* intercept. Time courses of the onset of inactivation were determined by plotting fractional inactivation ( $I_{\text{peak, pulse 2}} / I_0$ ) versus the conditioning pulse duration ( $\Delta t$ ), where *I*<sub>0</sub> is the maximum peak current amplitude. The inactivation time constants were then determined from the time courses of inactivation using the best-fit single exponential of the form  $y(t) = [y_0 + A e^{-t/\tau}]$ , where *A* is the amplitude,  $\tau$  is the conditioning pulse interval,  $\tau$  is the inactivation time constant, and *y*<sub>0</sub> is the *y* offset.

### Kinetic modeling

Kinetic modeling was based on the six-state kinetic model of NaChBac gating previously proposed by Kuzmenkin et al. (2004), which has been used by others to model interactions of sevoflurane and isoflurane with NaChBac (Barber et al., 2014; Sand et al., 2017). This gating scheme was modified to strictly allow closed-state recovery from inactivation, as described in Results and in the Online supplemental material, to globally simulate all key aspects of Nav gating examined experimentally. All kinetic simulations were performed in IonChannelLab (Santiago-Castillo et al., 2010). The objective of these simulations was to qualitatively account for all major voltage-dependent and kinetic features of a stereotypical prokaryotic Nav in the absence and presence of propofol. These features included the voltage dependencies of activation



and inactivation and the kinetics of activation, inactivation, deactivation, and recovery from inactivation. To generate modeled datasets, simulated currents were evoked in IonChannelLab using the experimental voltage protocols and analyzed in the same manner as experimentally observed currents. Rate constants were adjusted manually and kinetic parameters evaluated in an iterative process. Model parameters were first adjusted to approximate the control setting without anesthetic, then appropriately refined to develop a model of propofol modulation (Table S1).

### MD simulations and molecular docking

To discover potential propofol binding sites in Navs, we used an MD protocol, hereafter referred to as MD “flooding simulations.” In these flooding simulations, a single ion channel molecule is exposed to a large number of ligand molecules, a procedure that we have previously implemented to study the binding of the volatile anesthetics isoflurane and sevoflurane to NaChBac (Raju et al., 2013; Barber et al., 2014). Highly lipophilic ligands with large water/octanol partition coefficients like general anesthetics rapidly segregate into the lipid bilayer, resulting in a vanishingly small bulk solution concentration. Under these conditions, the near absence of anesthetic molecules in the aqueous compartment raises computational challenges, as binding events become extremely rare. This is in contrast to physiological conditions during the administration of volatile anesthetics, where the bulk solution concentration remains nearly constant because of the equilibrium between the aqueous phase in the blood stream and the gaseous phase in the lung alveoli (Eger et al., 1965). Accordingly, increasing the number of anesthetic molecules in the simulated system ensures that the concentration in the aqueous compartment remains within the appropriate range during the equilibrium phase of sampling. This approach also increases sampling of binding events between the anesthetic molecule and the molecular surface of the ion channel. Previous computational investigations of NaChBac using this method showed that general anesthetics can diffuse in and out of the pore in part because of their small size and the presence of fenestrations (Payandeh et al., 2011; Raju et al., 2013; Barber et al., 2014) and also identified isoflurane binding sites that were later corroborated by  $^{19}\text{F}$ -NMR saturation transfer difference spectroscopy experiments (Kinde et al., 2016). Thus, even a submicrosecond MD simulation is likely sufficient to explore all relevant protein cavities in the ion channel. To this end, we applied this computational method to study the interactions between propofol and NavMs, for which a full-length crystal structure is available, specifically focusing on putative isoflurane binding sites previously identified in NaChBac (Raju et al., 2013; Kinde et al., 2016).

MD flooding simulations were performed on the x-ray crystal structure of NavMs in the open conformation (PDB accession no. 5HVX; Sula et al., 2017) in a fully hydrated lipid bilayer using NAMD 2.10 (Phillips et al., 2005). The simulation system contained a total of ~122,000 atoms, which included a NavMs tetramer, 434 lipid molecules (POPC), 25,310 water molecules, 236 ions ( $\text{Cl}^-$  and  $\text{Na}^+$ ), and 145 propofol molecules. The ratio of water to propofol molecules was 174.5, yielding an initial bulk concentration of 0.32 M. The system was equilibrated through three consecutive 2-ns stages, in which position restraints on differ-

ent groups were progressively released. The CHARMM36 force field was used for the phospholipids and CHARMM27 for the protein (Lee et al., 2014). Propofol parameters were obtained from LeBard et al. (2012). To avoid aggregation of propofol molecules, indicative of low solubility, a short-range repulsive potential was included between drug molecule pairs, using the collective module of NAMD 2.12 (Phillips et al., 2005). Periodic boundary conditions were used, and the electrostatic potential was evaluated using the particle mesh Ewald method. The lengths of all bonds containing hydrogen were constrained with the SHAKE/RATTLE algorithm. Each system was maintained at a temperature of 300°K and pressure of 1 atm using the Langevin thermostat and barostat methods as implemented in NAMD 2.10. The rRESPA (reversible reference system propagator algorithm) multiple time step method was used, with a high-frequency time step of 2 fs and a low frequency time step of 4 fs. A trajectory of ~230 ns was collected for subsequent analysis.

Based on the simulation results, we defined binding regions for molecular docking calculations to obtain a set of optimal binding poses and to further analyze channel-propofol interactions. Docking of propofol was performed on the x-ray crystallographic structure of NavMs in the open state (PDB accession no. 5HVX; Sula et al., 2017). The protein structure and parameters were assigned using the Protein Preparation Wizard (Schrödinger; Sastry et al., 2013), and protonation states were assigned assuming a pH of 7.0. A minimization step was performed using the OPLS3 force field (Jorgensen et al., 1996; Harder et al., 2016); a threshold of 0.30 Å was used on the RMSD of the heavy atoms to assess convergence. Propofol structures and parameters were assigned using LigPrep (Schrödinger). For each binding site, a set of top scoring binding poses was then obtained using Glide-SP (Schrödinger; Friesner et al., 2006).

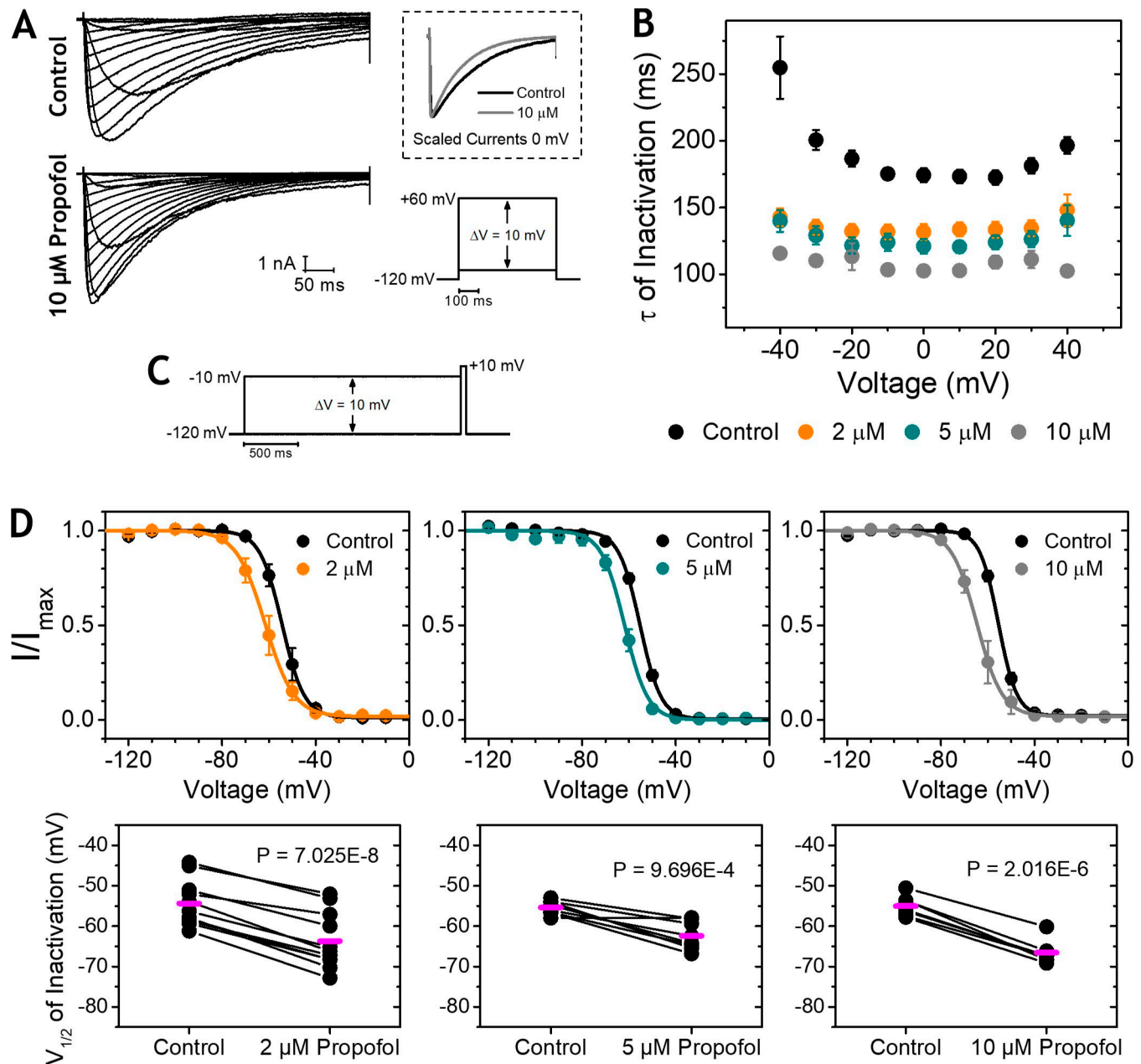
### Online supplemental material

Fig. S1 provides additional NaChBac WT inactivation gating parameters and also demonstrates representative curve fitting for inactivation kinetics. Fig. S2 provides additional NaChBac WT and T220A activation gating parameters. Fig. S3 shows representative curve fitting for NaChBac WT activation and deactivation kinetics. Fig. S4 examines the effects of propofol on the rate of NaChBac WT inactivation at -55 mV. Fig. S5 shows representative curve fitting for NavMs inactivation kinetics and provides additional information regarding activation and inactivation gating parameters. Fig. S6 explores other kinetic schemes to model NaChBac gating, and Fig. S7 investigates a scenario of propofol modulation that does not include effects on inactivation. Fig. S8 is a sequence alignment comparing the S4 to S6 segments of NaChBac and NavMs. Table S1 contains the kinetic model parameters used in IonChannelLab to describe NaChBac gating and modulation by propofol.

## Results

### Modulation of WT NaChBac inactivation properties

In general, anesthetics accelerate macroscopic inactivation in Navs, which could be a result of either accelerated entry into the inactivated state or slow open channel block. At 2, 5, and 10  $\mu\text{M}$ ,



**Figure 1. Modulation of NaChBac inactivation gating by propofol.** (A) Representative paired current families in the absence (control) and presence of 10  $\mu$ M propofol. Paired scaled  $I_{Na}$  currents at 0 mV (top) and the voltage protocol (bottom) are shown to the right. (B) Time constants ( $\tau$ ) of inactivation versus voltage. Propofol reduced  $\tau_{inactivation}$  at 2, 5, and 10  $\mu$ M ( $n = 15-19$ ) at all voltages ( $9.78E-10 < P < 0.015$ ), with the exception of the 10  $\mu$ M data point at -40 mV ( $P = 0.059$ ). (C) Pre-pulse inactivation voltage protocol. (D) Pre-pulse inactivation curves of control and with propofol at 2, 5, and 10  $\mu$ M ( $n = 7-11$ ). Corresponding paired midpoint voltages ( $V_{1/2}$ ) of inactivation are shown below. Means are indicated in magenta. Error bars indicate  $\pm$ SEM.

propofol consistently accelerated the decay of macroscopic WT NaChBac currents over a wide range of membrane potentials (Fig. 1, A and B). This current decay was well described by a single exponential function (Fig. S1, B and C). At voltages greater than -40 mV, where the time constant of inactivation demonstrated little to no voltage dependence, propofol exposure decreased the time constants uniformly (Fig. 1 B). At +20 mV, for instance, the time constant of inactivation was reduced  $24 \pm 3.9\%$ ,  $22 \pm 5.5\%$ , and  $33 \pm 2.5\%$  at 2, 5, and 10  $\mu$ M, respectively.

Anesthetics also generally induce parallel hyperpolarizing shifts of the pre-pulse inactivation curves in Navs (Covarrubias

et al., 2015), which points to a relative stabilization of the inactivated state. In WT NaChBac, we observed significant hyperpolarizing shifts of the pre-pulse inactivation curves without any changes in the corresponding effective gating charge of inactivation (Figs. 1 D and S1 A). At 2, 5, and 10  $\mu$ M, the changes in the midpoint voltage ( $V_{1/2}$ ) of inactivation compared with control were  $-9.33 \pm 0.67$ ,  $-7.02 \pm 1.29$ , and  $-11.51 \pm 0.65$  mV, respectively (Table 1). These shifts corresponded to a 25%, 29%, and 32% reduction in channel availability in the presence of 2, 5, and 10  $\mu$ M propofol, respectively, at the corresponding baseline midpoint voltage (Fig. 1 D).

Table 1. Effect of propofol on NaChBac and NavMs gating parameters

	NaChBac WT			NaChBac T220A	NavMs
	2 $\mu$ M	5 $\mu$ M	10 $\mu$ M	5 $\mu$ M	5 $\mu$ M
$\Delta V_{1/2}$ of activation (mV)	$-12.62 \pm 0.93$	$-9.82 \pm 1.82$	$-14.98 \pm 1.17$	$-14.16 \pm 0.93$	$-12.46 \pm 1.55$
$\Delta V_{1/2}$ of inactivation (mV)	$-9.33 \pm 0.67$	$-7.02 \pm 1.29$	$-11.51 \pm 0.65$	N/A	$-13.54 \pm 1.61$

Changes in the midpoints ( $V_{1/2}$ ) of activation and inactivation are evident at all concentrations and in all channels tested,  $P < 0.001$ , by paired samples  $t$  test.

To test whether these shifts were a result of an actual stabilization of the inactivated state, we examined recovery from inactivation at  $-120$  mV, a strongly hyperpolarized voltage that allows isolated investigation of the recovery process. At the same concentrations, propofol had no significant effect on the kinetics of recovery from inactivation (Fig. 2), which were all well described by a single exponential function. At  $10 \mu\text{M}$ , the time constant of recovery was  $1,075 \pm 208$  ms, compared with  $849 \pm 125$  ms for paired controls ( $P = 0.2433$ ). Overall, these results demonstrate that modulation of NaChBac inactivation by propofol does not involve stabilization of the inactivated state; they do not, however, eliminate the possibility of open pore block.

#### A non-inactivating NaChBac mutant demonstrates no evidence of pore block by propofol

Slow open channel blockers of voltage-gated ion channels induce time-dependent decay of the current, which reflects the time course of pore block (Armstrong, 1966, 1971; Shin et al., 2001; Wang et al., 2004; Barber et al., 2014; Sand et al., 2017). In NaChBac, however, interpretation of changes in this decay could be confounded by the presence of intrinsic inactivation. Thus, to directly determine whether propofol acts as a slow open channel blocker of NaChBac, we generated NaChBac T220A, a previously reported mutant that lacks macroscopic inactivation at baseline (Lee et al., 2012a). Examination of this non-inactivating mutant would allow direct observation of any pore blocking kinetics in the absence of confounding inactivation. Contrary to these expectations, however, there was no evidence of slow pore block, as  $5 \mu\text{M}$  propofol failed to induce any current decay (Fig. 3 A). Moreover, there was a  $16 \pm 7.4\%$  increase in the maximum peak current amplitude ( $P = 0.00614$ ; Figs. 3 B and S2 B), demonstrating that propofol does not act as a fast resting state pore blocker either. These results point to gating modulation as the basis for the acceleration of macroscopic current decay induced by propofol in WT NaChBac (Fig. 1 A, inset; and Fig. 1 B) rather than open pore block. Consistent with this conclusion and the hyperpolarizing shift of the pre-pulse inactivation curve, propofol also accelerated entry into the inactivated state (Figs. 1 and S4).

#### Modulation of NaChBac activation properties

In Navs, inactivation is inherently coupled to channel activation (Armstrong and Bezanilla, 1977; Armstrong, 1981, 2006; Aldrich and Stevens, 1987), and thus, effects on activation alone could account for changes seen in the voltage dependence and kinetics of inactivation. To evaluate the modulation of activation gating by propofol, we compared the conductance-voltage (G-V) rela-

tionships of WT and non-inactivating T220A NaChBac in the absence and presence of propofol. In both channels, propofol induced parallel hyperpolarizing shifts of the G-V curves at all concentrations (Fig. 4). In WT NaChBac, the changes in the  $V_{1/2}$  of activation compared with control were  $-12.62 \pm 0.93$ ,  $-9.82 \pm 1.82$ , and  $-14.16 \pm 0.93$  mV at 2, 5, and  $10 \mu\text{M}$  propofol, respectively (Fig. 4 A and Table 1). At baseline, NaChBac T220A demonstrates voltage-dependent activation that is more hyperpolarized compared with WT (Figs. 4 B and S3 B, left), which results from the elimination of inactivation. Nonetheless,  $5 \mu\text{M}$  propofol similarly induced a parallel hyperpolarizing shift in the G-V curve, corresponding to a change in the  $V_{1/2}$  of activation of  $-14.16 \pm 0.93$  mV, an effect that is also evident in the current-voltage (I-V) relationships (Fig. 3 B). This demonstrates that positive modulation of activation by propofol in NaChBac occurs in a manner that does not depend on the presence of inactivation and suggests that the propofol-induced acceleration of inactivation could result largely from promoting voltage-dependent activation and pore opening.

To investigate the kinetic basis of this positive modulation, we determined the time constants of deactivation from tail current relaxations and the time constants of activation from the rising phase of the inward  $\text{Na}^+$  currents (Figs. 5 and S4). As is typical for voltage-gated ion channels, deactivation dominates at hyperpolarized voltages and activation dominates at depolarized voltages, with the measured time constants meeting near the  $V_{1/2}$  of activation. At 2 and  $5 \mu\text{M}$ , propofol failed to induce changes in the time constants of deactivation in WT NaChBac and required a high concentration ( $10 \mu\text{M}$ ) to produce observable slowing (Fig. 5 A, bottom; and Fig. 5 C). In contrast, all concentrations of propofol reduced the time constants of activation (Fig. 5 A, top; and Fig. 5 C). Very similar effects were seen in NaChBac T220A (Fig. 5, B and D). These results demonstrate that the propofol-induced hyperpolarizing shift of the G-V curve is governed primarily by the acceleration of activation gating.

#### Modulation of NavMs activation and inactivation properties by propofol

Results in NaChBac show that propofol does not act via open pore block and has favorable effects on both voltage-dependent activation and inactivation gating. We next asked whether the effects are conserved in NavMs, a prokaryotic Nav for which a full-length crystal structure was recently determined (Sula et al., 2017). Compared with NaChBac, NavMs displays gating kinetics one order of magnitude faster and has a more hyperpolarized voltage dependence (Ulmschneider et al., 2013). NavMs also exhibits high selectivity for  $\text{Na}^+$  (Ulmschneider et al., 2013;



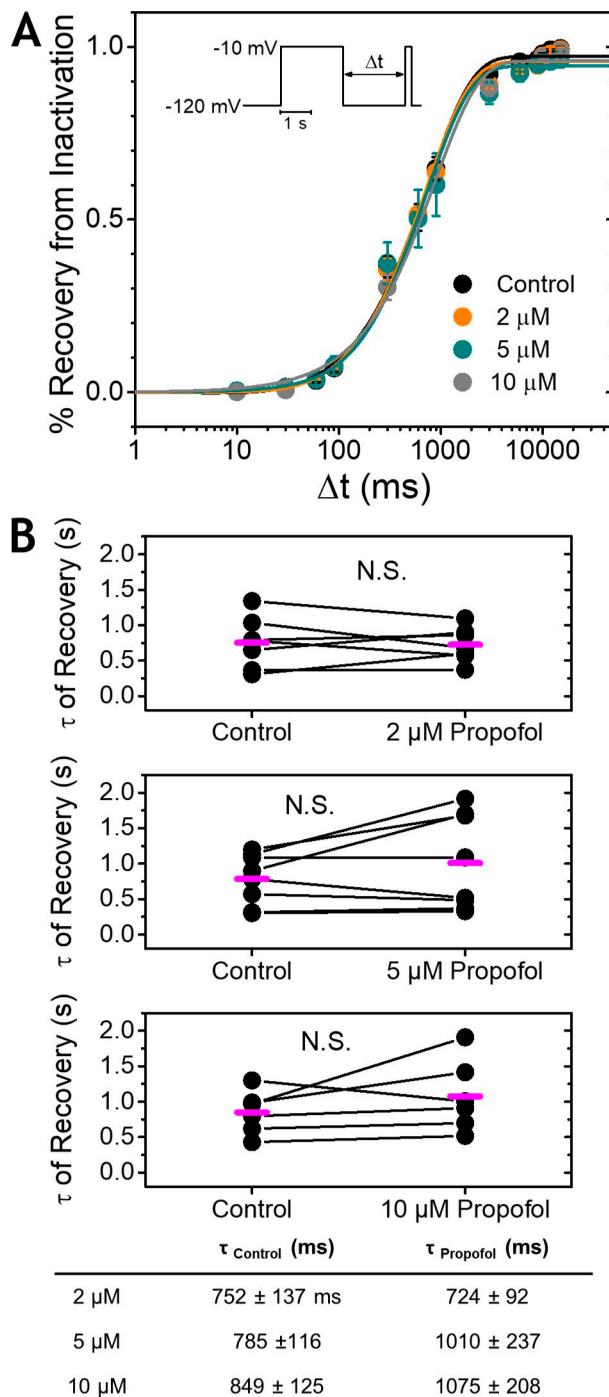


**Figure 2. Propofol does not affect recovery from inactivation in NaChBac.** (A) Time courses of recovery from inactivation. (B) Paired time constants ( $\tau$ ) of recovery in the absence (control) and presence of 2, 5, and 10  $\mu$ M propofol ( $n = 6-8$ ). Inset shows the voltage protocol. Means are indicated in magenta. Error bars indicate  $\pm$ SEM.

Naylor et al., 2016) and contains a common binding site for Nav antagonists in the central pore (Bagn  ris et al., 2014; Buyan et al., 2018). Despite any functional and structural differences, however, 5  $\mu$ M propofol modulated NavMs gating parameters in a manner largely mirroring its effects on NaChBac. These effects include accelerated Na<sup>+</sup> current decay (Fig. 6, A and C; and Fig. S5, A and B), parallel hyperpolarizing shifts of both the G-V and pre-

pulse inactivation curves (Fig. 6, D and E; and Fig. S5 C), and no effect on recovery from inactivation (Fig. 6 F). Thus, modulation by propofol is conserved in both NaChBac and NavMs, suggesting that fundamentally similar interactions govern these effects and indicating that NavMs provides a robust system for future structural investigations into general anesthetic action.

#### Kinetic modeling of prokaryotic Nav gating requires closed-state recovery from inactivation

We next used computer simulations based on a kinetic model of NaChBac gating previously proposed by Kuzmenkin et al. (2004) to develop a model of propofol action on prokaryotic Navs. This kinetic model of NaChBac gating assumes a sequential six-state gating scheme, with channels making voltage-dependent transitions between the closed and open states and the open and inactivated states (Fig. S6 A). Importantly, it assumes that channel inactivation is strictly coupled to pore opening and that inactivated channels must recover from inactivation via the open state. Although the linear model largely reproduces the major features of NaChBac gating, it does not adequately model recovery from inactivation at -120 mV, yielding a time constant of recovery close to experimental values ( $\sim 800$  ms) but also a time course of recovery from inactivation with a considerable y offset (Fig. S6 C). This y offset indicates significant channel reopening from the inactivated state and produces simulated current families that exhibit substantial sustained currents that are not observed experimentally (Fig. S6 B, top). Slowing the rate constant of recovery from inactivation ( $\beta_2$ ) by an order of magnitude was able to minimize the sustained current (Fig. S6 B, middle) but was unable to reproduce the experimentally observed time course of recovery from inactivation (Fig. S6 C).

To resolve these discrepancies, we introduced an alternative pathway of recovery from inactivation that does not allow channel reopening (Fig. 7 A, Control). Instead, inactivated channels preferentially return to the resting/closed state from the inactivated state. In other words, they must first close ( $I_o \rightarrow I_c$ ) before they are able to return to the pre-open closed state ( $I_c \rightarrow C$ ). Recovery coupled to deactivation has previously been proposed by Kuo and Bean (1994) to describe Nav recovery from inactivation in hippocampal CA1 neurons. The model proposed here demonstrates inactivation pathway hysteresis, whereby separate pathways are taken to enter and leave the inactivated state. In response to a depolarizing step, the Navs activate, open, and enter the inactivated state ( $C \rightarrow O \rightarrow I_o$ ), which appears absorbing if the depolarized voltage is held. After hyperpolarization, the inactivated Navs close and enter the inactivated-closed state ( $I_o \rightarrow I_c$ ) before returning to the pre-open closed state ( $I_c \rightarrow C$ ), thereby completing the open-inactivation-recovery cycle. A similar model of activation-coupled inactivation has been described for K<sup>+</sup> channels exhibiting C-type inactivation (Tilegenova et al., 2017). The proposed model of Nav gating with inactivation pathway hysteresis closely described prokaryotic Nav gating kinetics while simultaneously allowing complete inactivation and sufficiently fast recovery from inactivation (Table S1; Fig. S6 B, bottom; and Fig. S6 C). We also found that measurements of the rate of inactivation in NaChBac land closely to the trajectory of the inward Na<sup>+</sup> current, which re-

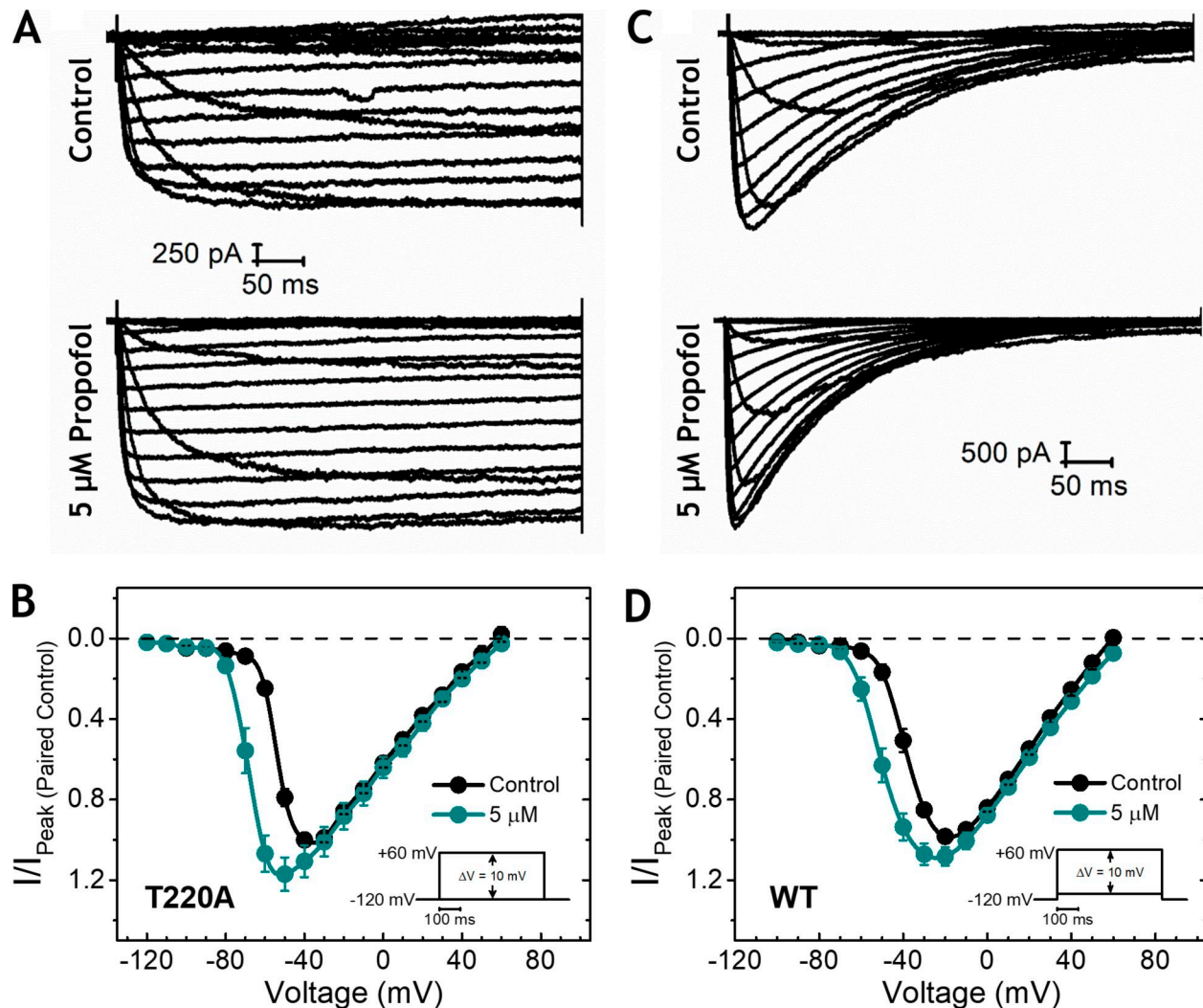


Figure 3. **Propofol does not act as a pore blocker in a non-inactivating NaChBac mutant.** (A) Representative paired current families evoked from NaChBac T220A in the absence (control) and presence of 5  $\mu$ M propofol. (B) Normalized current-voltage (I-V) relationships of control and 5  $\mu$ M propofol from NaChBac T220A. Currents were normalized to the maximum peak current of the paired control for each cell ( $n = 11$ ). Inset shows the voltage protocol. (C and D) Representative paired current families (C) and normalized I-V relationships from NaChBac WT (D;  $n = 15$ ) are shown to provide a side-by-side comparison. Error bars indicate  $\pm$ SEM.

flects the time-dependent change in open probability at the corresponding voltage, thus unambiguously demonstrating that inactivation in NaChBac is strictly coupled to pore opening (Fig. S4 B; Fineberg et al., 2012).

#### Propofol primarily accelerates voltage-dependent activation to promote inactivation in prokaryotic Navs

Using the model of Nav gating with inactivation pathway hysteresis, we next developed a model of propofol modulation based on the experimentally observed results. First, we determined whether positive modulation of activation alone could be sufficient to explain the promotion of inactivation (Fig. S7 A), a feasible scenario when inactivation is strictly coupled to pore opening. A 1.7-fold acceleration of the forward activation rate constant  $\alpha_1$  combined with a modest 1.25-fold slowing of the backward deactivation rate constant  $\beta_1$  was sufficient to qualitatively reproduce propofol-induced hyperpolarizing shifts of the G-V ( $\Delta V_{1/2 \text{ Activation}} = -8.68$  mV) and pre-pulse inactivation

( $\Delta V_{1/2 \text{ Inactivation}} = -8.23$  mV) curves (Fig. S7, B and C). However, under these model conditions, macroscopic inactivation was not accelerated compared to control at strongly depolarized voltages (Fig. S7 D), whereas propofol uniformly decreased experimentally derived time constants of inactivation over the full range of membrane potentials studied (Fig. 1 B). Thus, to globally account for all voltage-dependent and kinetic properties, it was necessary to assume a 1.4-fold acceleration of the forward inactivation rate constant  $\alpha_2$  in addition to the changes in  $\alpha_1$  and  $\beta_1$  above. Model parameters can be found in Table S1. These assumptions were sufficient to closely account for all aspects of propofol modulation of NaChBac and NavMs inactivation (Fig. 7) and activation (Fig. 8) gating. The kinetic modeling therefore supports the experimental findings that propofol primarily modulates voltage-dependent activation, with separate but more modest effects on voltage-dependent inactivation, and ultimately inhibits prokaryotic Navs by promoting activation-coupled inactivation.



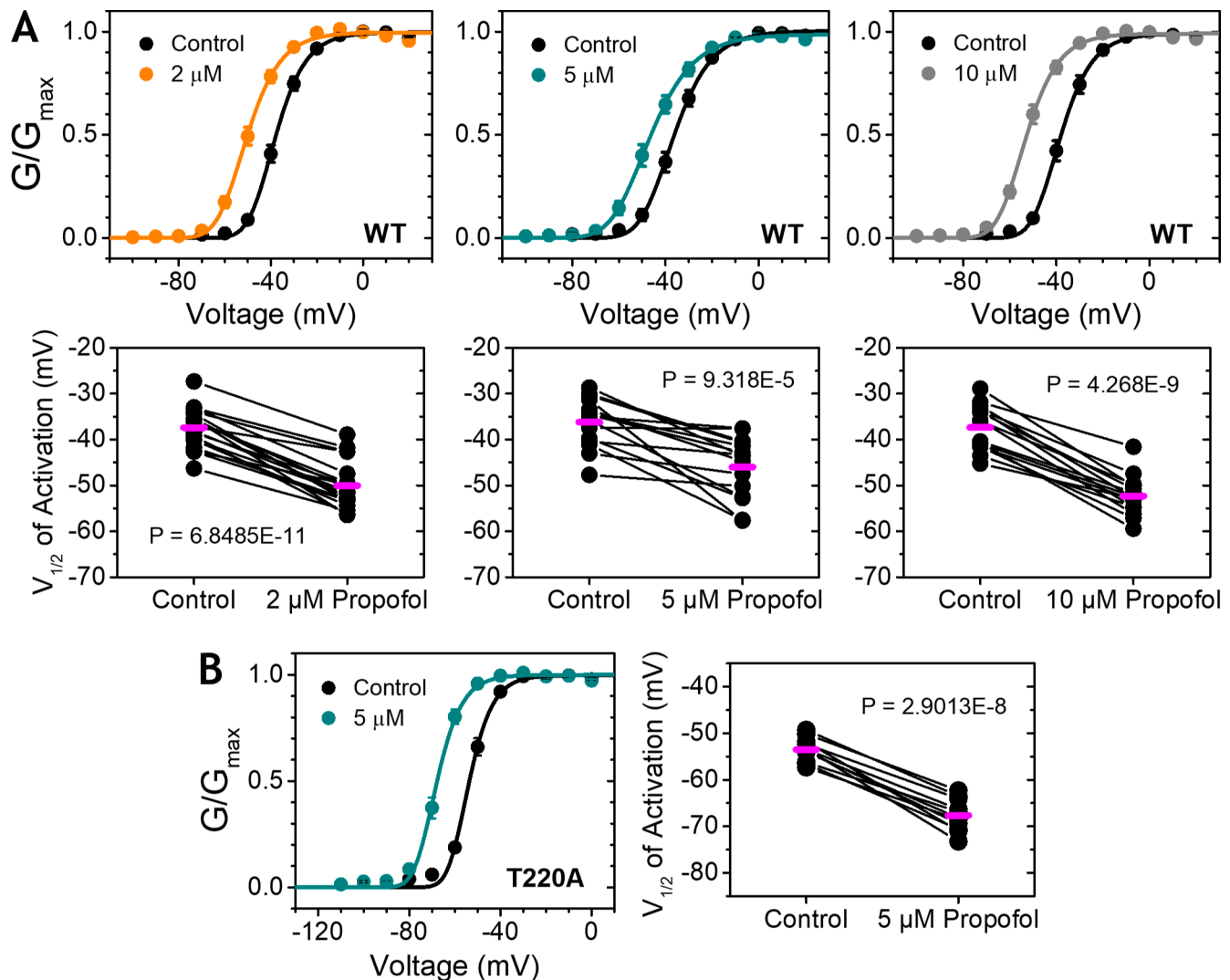


Figure 4. **Propofol induces a relative stabilization of the open state in both WT and non-inactivating NaChBac.** (A) WT ( $n = 15\text{--}19$ ): Normalized peak G-V relationships in the absence (control) and presence of 2, 5, and 10  $\mu\text{M}$  propofol, with corresponding paired  $V_{1/2}$ s of activation shown below. (B) T220A ( $n = 11$ ): Normalized G-V relationships of control and with 5  $\mu\text{M}$  propofol (left) and corresponding paired  $V_{1/2}$ s of activation (right). Means are indicated in magenta. Voltage protocols are the same as those in Fig. 3. Error bars indicate  $\pm\text{SEM}$ .

## Discussion

Despite widespread clinical use, the mechanism of action of the intravenous general anesthetic propofol is not completely understood. This study provides mechanistic insight into the biophysical and molecular basis of interactions between propofol and two prokaryotic Navs, NaChBac and NavMs. These prokaryotic Navs share fundamental properties with eukaryotic Navs and thus serve as powerful models to investigate the mechanisms of propofol action on Navs. Here, we show that propofol (a) hyperpolarizes the pre-pulse inactivation curve, (b) accelerates the rate of macroscopic inactivation, (c) does not affect recovery from inactivation at a strongly hyperpolarized voltage, (d) hyperpolarizes the G-V curve in both the presence and absence of channel inactivation, (e) does not induce slow or fast open pore block, (f) accelerates the rate of macroscopic current activation with only minor effects on deactivation, and (g) induces nearly identical effects in both NaChBac and NavMs. Using kinetic modeling, we determined that the net inhibitory effect of propofol on

prokaryotic Navs can be explained by significant catalytic action on voltage-dependent activation gating and, separately, modest catalytic action on slow voltage-independent inactivation gating. These two distinct effects together ultimately promote activation-coupled inactivation, which, as MD simulations of both NavMs and NaChBac suggest, might be a result of interactions with the ion channel's gating apparatus (Wang et al., 2018).

### Propofol is a positive gating modulator of prokaryotic Navs that promotes activation-coupled inactivation

It has been shown that propofol acts as a positive modulator of various ion channels (Jayakar et al., 2013, 2014; Li et al., 2016; Ton et al., 2017), which are presumably responsible for both the desired endpoints and adverse effects of general anesthesia. Propofol depresses brain activity in part through the positive modulation of ionotropic GABA<sub>A</sub> receptors (Orser et al., 1994; Belelli et al., 1999; Jurd et al., 2003; Zecharia et al., 2009; Woll et al., 2015). Pain and irritation caused by the administration of

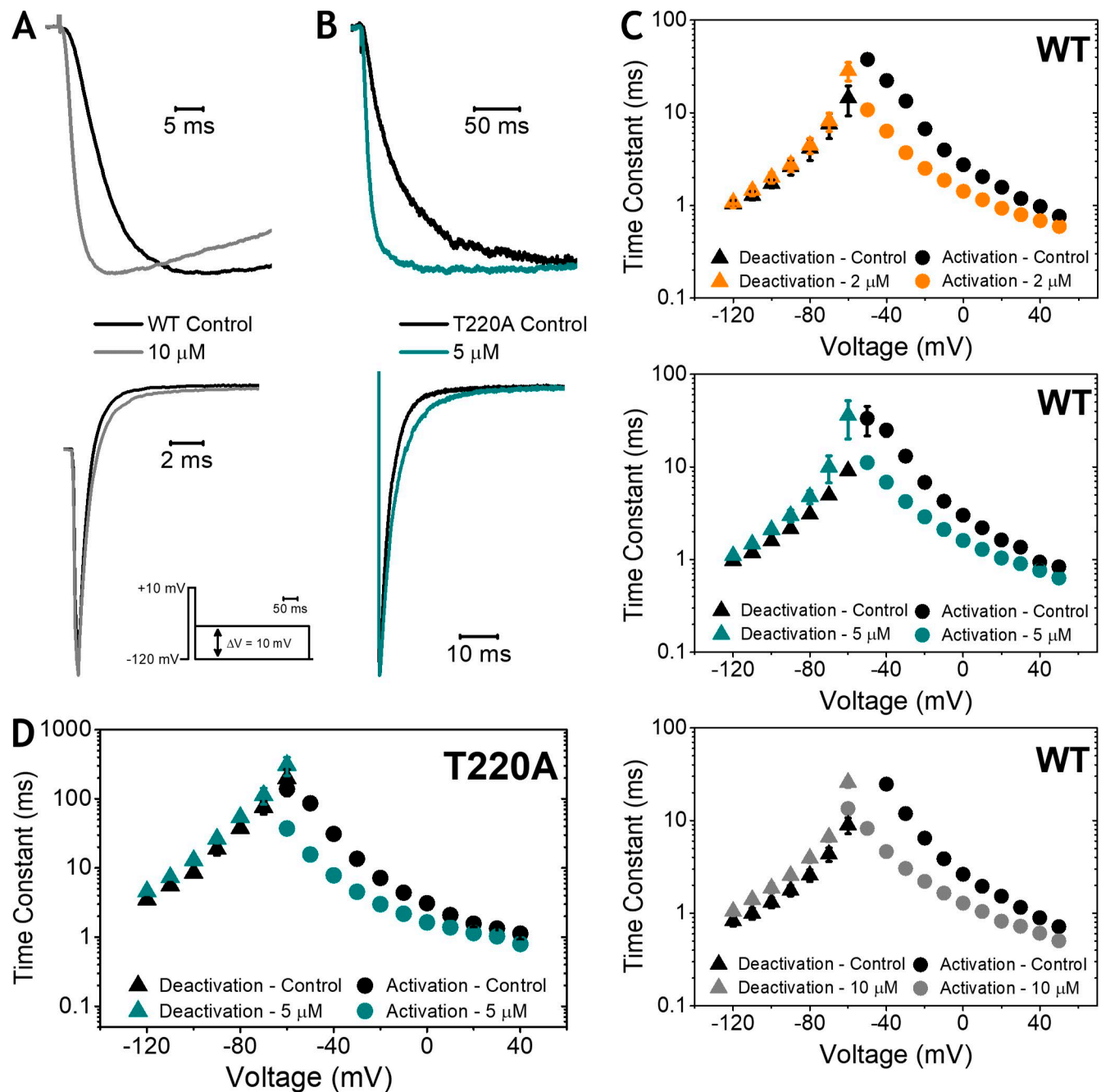


**Figure 5. Propofol preferentially accelerates macroscopic activation in both WT and non-inactivating NaChBac.** (A and B) Representative scaled  $I_{Na}$  currents at  $-40$  mV (top) and deactivation currents at  $-120$  mV (bottom) evoked from WT (A) and T220A (B), in the absence and presence of 10 or 5  $\mu$ M propofol, respectively. Inset shows the deactivation voltage protocol used for both WT and T220A.  $I_{Na}$  currents were evoked using the voltage protocols shown in Fig. 3 B. (C and D) Time constants ( $\tau$ ) of activation (circles, right side) and deactivation (triangles, left side) versus voltage. Propofol reduced  $\tau_{Activation}$  in WT ( $n = 15-19$ ) and T220A ( $n = 10$ ) at all concentrations and voltages shown compared with control ( $2.74E-8 < P < 0.035$ ), with the exception of T220A at  $+40$  mV ( $P = 0.10$ ). In WT ( $n = 5-6$ ), 2 and 5  $\mu$ M propofol did not increase  $\tau_{Deactivation}$ , except for 2  $\mu$ M at  $-60$  mV ( $P = 3.40E-4$ ); 10  $\mu$ M increased  $\tau_{Deactivation}$  at all voltages shown ( $5.47E-4 < P < 0.015$ ). In T220A ( $n = 6$ ), 5  $\mu$ M propofol increased  $\tau_{Deactivation}$  ( $4.30E-4 < P < 0.035$ ), with the exception of  $-110$  and  $-70$  mV ( $P = 0.10$  and  $0.093$ , respectively). Error bars indicate  $\pm$ SEM. In most cases, error bars are smaller than symbols.

propofol are likely mediated by activation of TRPA1 channels via a binding pocket formed by residues of the S5, S6, and first pore helix (Ton et al., 2017), and recent photoaffinity labeling studies point to sites in the S6 helix that may also contribute to the ability of propofol to activate TRPA1 channels (Woll et al., 2017b). Moreover, as in TRPA1 channels, sevoflurane and propofol also

positively modulate voltage-gated  $K^+$  channels (Woll et al., 2017a; Barber et al., 2012; Liang et al., 2015; Bu et al., 2018).

In our investigations, we discovered that propofol also sensitizes prokaryotic Navs to changes in membrane potential, an effect that is evident in both the presence and absence of inactivation (Fig. 4). Ultimately, however, propofol inhibits these

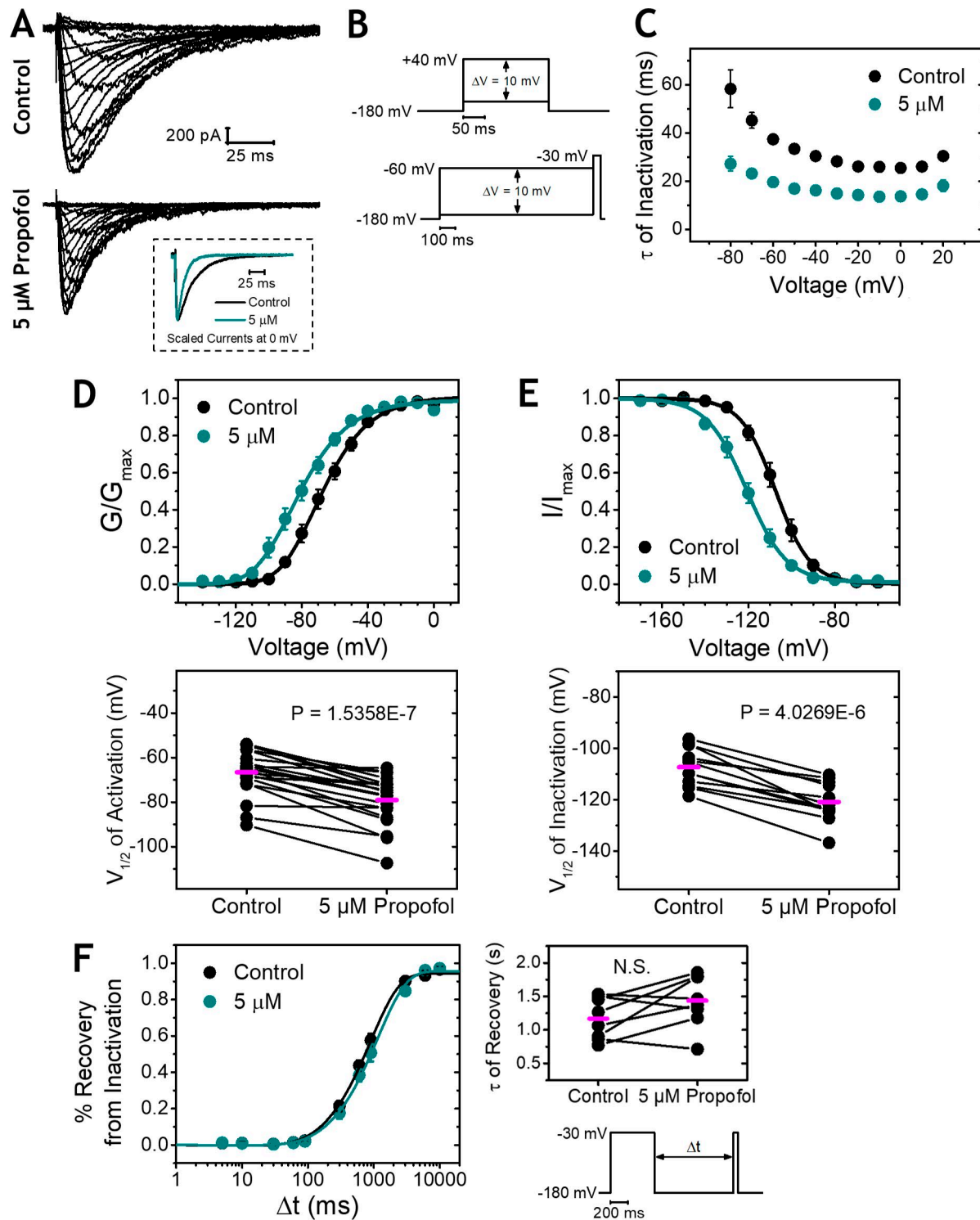


**Figure 6. Modulation of gating by propofol is conserved in NavMs.** (A) Representative paired current families evoked from NavMs in the absence (control) and presence of 5  $\mu\text{M}$  propofol. Inset shows representative paired scaled  $I_{\text{Na}}$  currents at 0 mV. (B) Voltage protocols for voltage-dependent activation (top) and pre-pulse inactivation (bottom). (C) Time constants ( $\tau$ ) of inactivation versus voltage ( $n = 20$ ). 5  $\mu\text{M}$  propofol reduced  $\tau_{\text{inactivation}}$  at all voltages shown ( $3.66\text{E-}9 < P < 0.002$ ). (D and E) Normalized peak  $G$ - $V$  relationships (D;  $n = 20$ ) and normalized pre-pulse inactivation curves (E;  $n = 12$ ) of control and with 5  $\mu\text{M}$  propofol. Corresponding paired  $V_{1/2}$ s of activation and inactivation are shown below. Means are indicated in magenta. (F) Time course of recovery from inactivation in the absence and presence of 5  $\mu\text{M}$  propofol (left). Corresponding paired time constants ( $\tau$ ) of recovery from inactivation (top),  $\tau_{\text{Control}} = 1170 \pm 109$  ms,  $\tau_{5 \mu\text{M}} = 1436 \pm 136$  ms ( $n = 8$ ), and the voltage protocol (bottom) are shown to the right. Error bars indicate  $\pm$  SEM.

Navs (Fig. 1 D) because inactivation is strictly coupled to activation and pore opening. In the presence of open-state inactivation, therefore, entry into the inactivated state is governed

by the voltage-dependent open probability (Fineberg et al.,



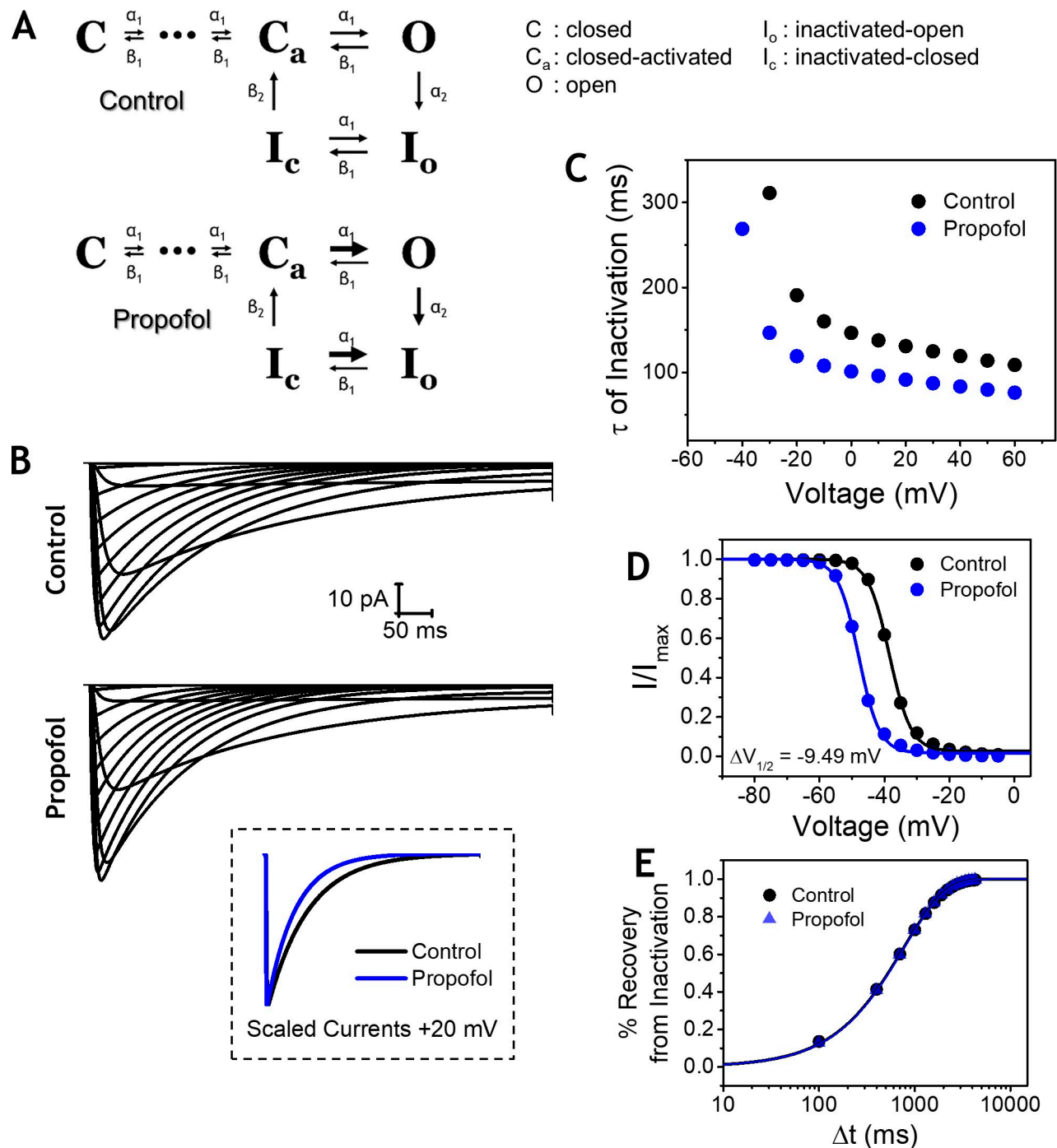


Figure 7. **Kinetic modeling of NaChBac inactivation properties.** (A) Proposed kinetic scheme in the absence (control) and presence of propofol. Model parameters are given in Table S1. (B–E) IonChannelLab simulation results of the proposed kinetic schemes. Simulated current families in the absence and presence of propofol (B). Inset shows scaled currents at +20 mV. Time constants ( $\tau$ ) of inactivation versus voltage of control and with propofol (C). Pre-pulse inactivation curves (D) and recovery from inactivation time courses (E) in the absence and presence of propofol.

2012). Consistent with this premise, kinetic modeling demonstrated that the primary effect of propofol is to promote activation by accelerating the forward voltage-dependent activation rate constant (Figs. 7, 8, and S7). This effect alone accounts for the propofol-induced hyperpolarizing shifts of the G-V and pre-pulse inactivation curves. Promotion of activation alone does not, however, account for the uniform acceleration of the time constants of inactivation (Figs. 1 B and S6 D), strongly

arguing in favor of a multimodal effect. Nonetheless, it is the hyperpolarized pre-pulse inactivation curve that ultimately dictates inhibition of the inward  $Na^+$  current by reducing channel availability.

#### Shared features between propofol and local anesthetics

Previous studies have suggested that propofol might act as a pore blocker that stabilizes the inactivated state of Navs, much

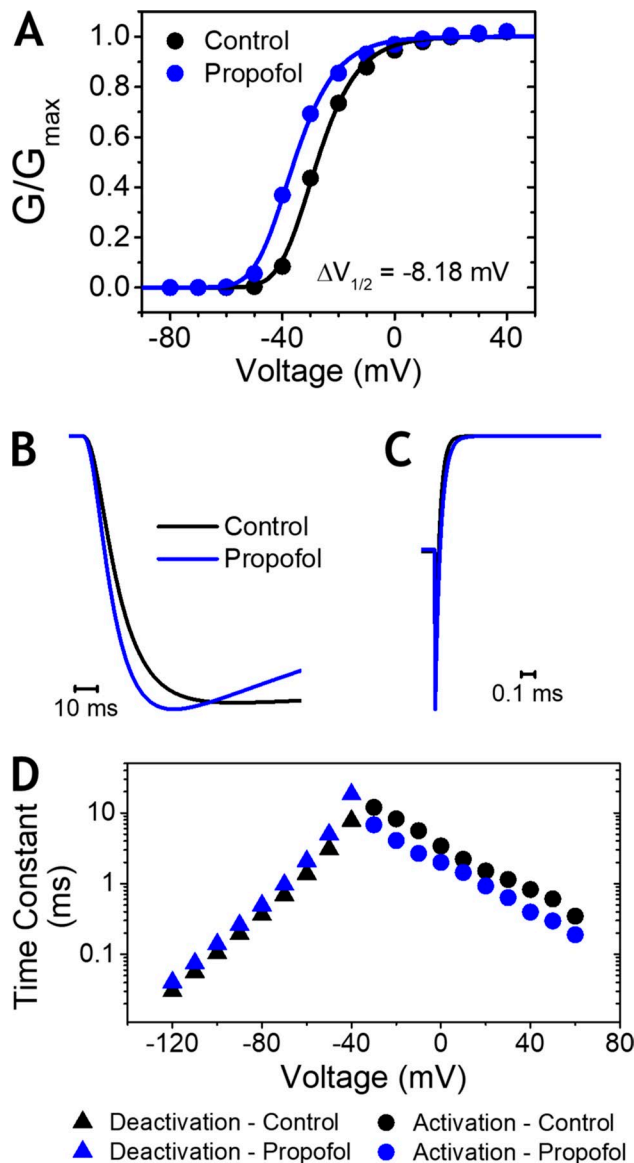


Figure 8. **Kinetic modeling of NaChBac activation properties.** Model parameters are the same as in Fig. 7 and are given in Table S1. (A) Peak G-V relationships in the absence (control) and presence of propofol. (B and C) Simulated, scaled activation currents at -40 mV (B) and deactivation tail currents at -120 mV (C) of control and with propofol. (D) Time constants of activation (circles, right side) and deactivation (triangles, left side) versus voltage, in the absence and presence of propofol.

like local anesthetics (Haeseler et al., 2001; Ouyang et al., 2003; Stoetzer et al., 2016). However, the reported effects, namely hyperpolarization of the steady-state inactivation curve, reduction of peak current amplitude, and slowed recovery from inactivation, could all be attributed to more favorable voltage-dependent activation. This possibility arises from the inherent coupling of inactivation to voltage-dependent activation, a shared property of many voltage-gated ion channels. As a consequence, if voltage-dependent activation is hyperpolarized, steady-state inactivation is necessarily hyperpolarized. Thus, within the range of voltages over which the Nav undergoes steady-state inactivation, the peak current amplitude is reduced, and recovery from inactivation is slowed.

Although this pattern of changes might at first glance resemble local anesthetic-induced stabilization of the inactivated state, our data provide a viable alternative explanation.

At strongly hyperpolarized voltages, propofol does not slow recovery from inactivation and negligibly slows deactivation in NaChBac. Propofol therefore does not stabilize the inactivated or open states. Moreover, in the absence of channel inactivation, neither instantaneous peak current amplitude reduction nor blocking kinetics was observed, which is inconsistent with a mechanism involving fast resting state or slow open pore block, respectively (Lee et al., 2012a; Goldschen-Ohm and Chanda, 2014). Hence, propofol does not act on prokaryotic Navs via classical local anesthetic mechanisms, namely the guarded and modulated receptor hypotheses (Strichartz, 1973; Hille, 1977; Goldschen-Ohm and Chanda, 2014). Nonetheless, propofol, the local anesthetics lidocaine and benzocaine, and the lidocaine derivative ranolazine all accelerate current decay and induce hyperpolarizing shifts of the G-V and pre-pulse inactivation curves in WT NaChBac (Figs. 1 and 4; Lee et al., 2012a,b). Resembling the mechanisms of propofol action proposed here, Lee et al. (2012b) suggested that local anesthetics may promote entry into the inactivated state. Like propofol, lidocaine also does not affect recovery from inactivation in NaChBac. Notably, however, propofol and lidocaine differ in that lidocaine induces robust fast resting state block of the non-inactivating T220A NaChBac mutant (Lee et al., 2012a) whereas propofol does not (Figs. 3 A and S3 B). The dissociation of pore blocking action from effects on voltage-dependent gating is consistent with a multisite and multimodal hypothesis of anesthetic action. Although propofol and local anesthetics appear to diverge with regard to pore blocking mechanisms, they may share overlapping allosteric sites near and in the pore that are associated with effects on gating.

#### Shared features between propofol and halogenated volatile anesthetics

Despite significant differences in chemical structure, the effects of halogenated volatile anesthetics on NaChBac share many features with those of propofol and local anesthetics. Ouyang et al. (2007) first investigated the modulation of NaChBac by isoflurane and proposed a mechanism of inhibition resembling that of local anesthetics. Their results appeared consistent with state-dependent interactions: stabilization of the inactivated state and open pore block (see above). We previously reported that sevoflurane also inhibits NaChBac via a mechanism that combines favorable voltage-dependent activation and inactivation gating with open pore block (Barber et al., 2014). Interestingly, sevoflurane modestly destabilizes the inactivated state by accelerating recovery from inactivation. More recently, Sand et al. (2017) revisited the modulation of NaChBac by isoflurane, using kinetic modeling to propose a mechanism of inhibition by isoflurane that involves increased forward activation and inactivation rate constants. Our results with propofol led to a similar conclusion in NaChBac and NavMs, which is further supported by semiquantitative global kinetic simulations based on an extended state model that includes inactivation pathway hysteresis (Figs. 7 A and S6). Our experiments additionally exclude the presence of fast or slow open pore block and demonstrate that

propofol has negligible effects on recovery from inactivation and deactivation kinetics.

Collectively, the similarities between the actions of local and general anesthetics on prokaryotic Navs suggest that these ion channels feature multiple structural pathways and binding pockets that allow promiscuous but functionally important interactions with a group of diverse chemical compounds that generally share significant hydrophobic character. It is particularly interesting that anesthetics also often have sensitizing effects on gating through catalytic action or stabilization of activated/open states in other related tetrameric ion channels, including K<sup>+</sup> and TRPA channels (Woll et al., 2017a, 2017b; Arcisio-Miranda et al., 2010; Barber et al., 2012; Liang et al., 2015; Ton et al., 2017). This observation points to the possibility of shared and/or related binding sites in other ion channels as well.

### Potential propofol binding sites and modulatory mechanisms in NavMs

Definitively linking functional observations to a discrete set of well-defined binding sites would require extensive investigation and validation that are beyond the scope of the present study. However, some qualitative conclusions can be drawn based on available information, specifically regarding the binding of isoflurane to NaChBac (Raju et al., 2013). Given the many shared features of NaChBac's functional response to both isoflurane and propofol (Sand et al., 2017) and the strikingly similar responses of NaChBac and NavMs to propofol, these general anesthetics could share binding sites in prokaryotic Navs. Although largely speculative, this hypothesis is consistent with many independent observations of distinct general anesthetics across many ion channels of the 6TM family, as discussed previously.

To this end, we performed MD flooding simulations on NavMs (see Materials and methods) and assessed the locations of two putative isoflurane binding sites previously identified in NaChBac (Raju et al., 2013) for potential propofol binding: an extracellular pocket near the selectivity filter at the intersubunit interface and an intracellular pocket lined by the S4–S5 linker and S6 helix of neighboring subunits (Fig. 9 A). Monitoring the distances between propofol molecules and the side chains lining these binding sites during the simulation showed that there is steric complementarity between the propofol molecule and both binding sites and that binding at each of these locations occurs within a few tens of nanoseconds (Fig. 9 F). Although this does not allow us to draw conclusions about occupancy of these sites under physiological conditions, it shows that binding is possible. We then performed molecular docking to conduct a more detailed analysis of the propofol-NavMs interactions at these locations and identified the side chains in NavMs that are most likely to be in contact with propofol (Fig. 9, C and E).

At the S4–S5 linker, the propofol molecule fits snugly in a pocket that is almost perfectly complementary in shape to the anesthetic molecule (Fig. 9 D). Binding in this pocket seems to be dominated by nonpolar interactions; the side chains lining the binding pocket are all hydrophobic in character except for T225. The propyl and phenyl moieties of propofol establish extensive interactions with the side chains of V131, V134, N212, and M222 (Fig. 9 E), and in several binding poses, the propofol hydroxyl

group is positioned to form a hydrogen bond with the main chain carbonyl of G130. As the S4–S5 linker is critical for electromechanical coupling and channel gating (Long et al., 2005; Payandeh et al., 2011), identification of a potential binding site at the S4–S5 linker is consistent with experimental findings that propofol acts as a gating modulator of prokaryotic Navs. Propofol binding on the extracellular side of the pore domain occurred near the selectivity filter at the interface between adjacent subunits (Fig. 9 B). Here, the propofol molecule established extensive contacts with R186 and N190 as well as K166 of the adjacent subunit (Fig. 9 C). Propofol might also interact with the outer pore region to modulate the equilibrium between conductive and non-conductive conformations of the selectivity filter, which has been implicated in slow inactivation in both eukaryotic Navs and in NaChBac (Xiong et al., 2003; Pavlov et al., 2005). Identification of these two potential binding sites lends additional support to a multisite and multimodal hypothesis of propofol action. In the companion article, Wang et al. (2018) characterized propofol binding at the S4–S5 linker and at a number of other candidate binding sites using <sup>19</sup>F-NMR. Further investigation will be required to validate the functional relevance of these sites to propofol action in Navs.

Although it is not possible to definitively link the binding pocket formed by the S4–S5 linker and S6 segment to the modulation of activation and inactivation gating based on the results presented here, it is very likely that interactions at this location are involved, given that these regions are highly conserved in both NaChBac and NavMs (Fig. S8) and given their shared functional modulation by propofol. This hypothesis is also strongly supported by previous work investigating the action of volatile general anesthetics on structurally related ion channels, such as NaChBac, Kv, and TRP channels (Woll et al., 2017a, 2017b; Barber et al., 2012, 2014; Zhang et al., 2013; Liang et al., 2015; Kinde et al., 2016; Ton et al., 2017; Bu et al., 2018). Toward linking our findings to mechanisms of general anesthetic action in eukaryotic Navs, this binding pocket near the S4–S5 linker is especially intriguing in light of the recent cryo-EM structure of Nav1.4 from electric eel *Electrophorus electricus* (EeNav1.4) in complex with the  $\beta$ 1 subunit (Yan et al., 2017). In the structure, the III–IV cytoplasmic linker containing the LFM fast inactivation motif is found wedged into the corner enclosed by the S4–S5 linkers and S6 of domains III and IV, precisely the location of the putative propofol binding pocket in NavMs. If the III–IV cytoplasmic linker mediates fast inactivation through an allosteric mechanism that induces pore closure, propofol may mimic the inactivation gate when it binds to this pocket, thereby promoting entry into the inactivated state.

### Limitations of the model system and kinetic modeling

It is uncertain whether the mechanism of propofol action on NaChBac and NavMs proposed here can be completely extrapolated to eukaryotic Navs. Several experimental observations, however, are consistent with fundamental aspects of anesthetic mechanisms: (1) local and general anesthetics universally hyperpolarize the voltage dependence of inactivation gating in Navs (Hille, 1977; Bean et al., 1983; Ouyang et al., 2003, 2007, 2009; OuYang and Hemmings, 2007; Lee et al., 2012a; Barber et al., 2014; Sand et al., 2017), (2) local anesthetics are able to



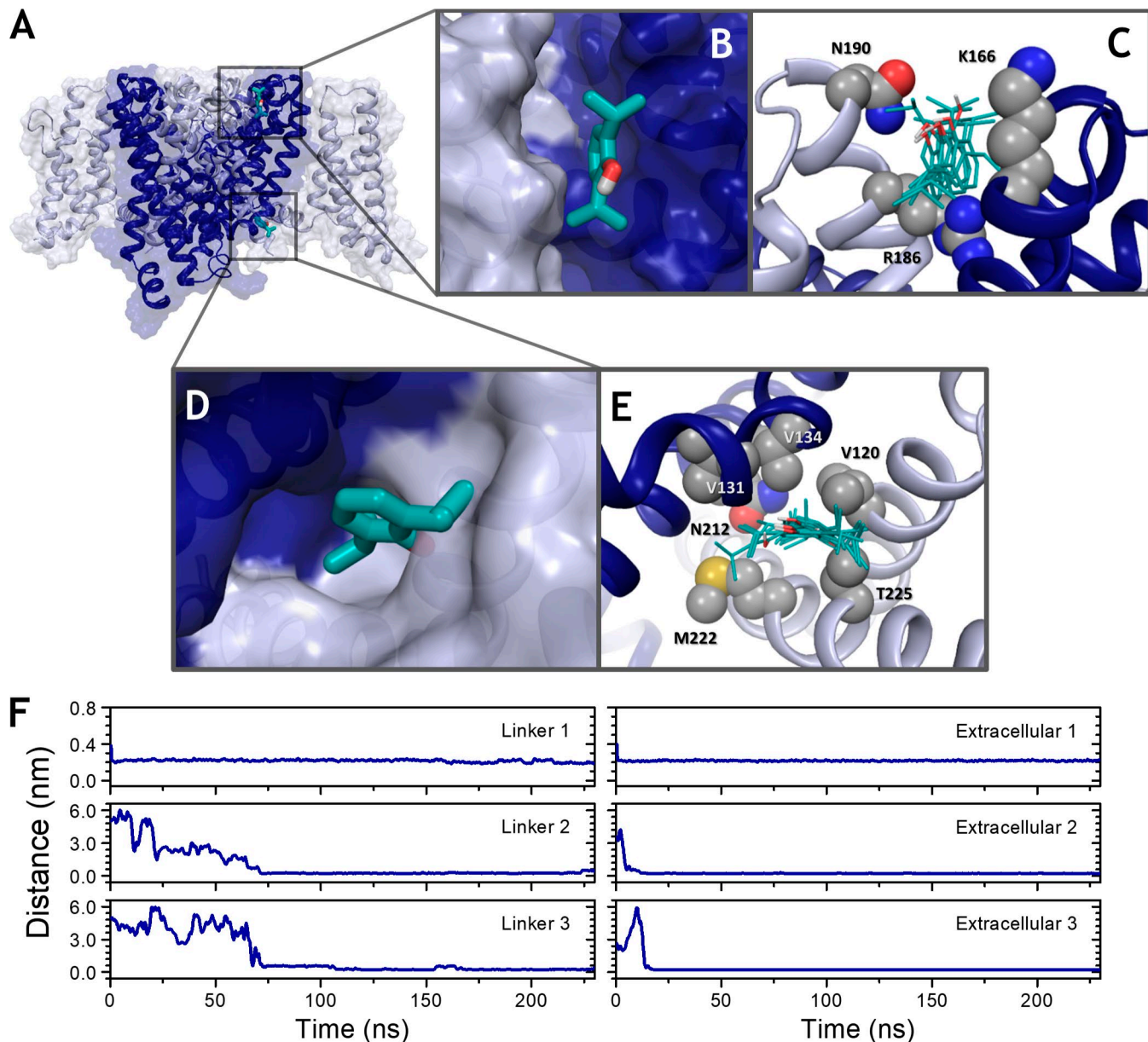


**Figure 9. MD simulations and molecular docking in NavMs.** (A) Side view of potential propofol binding sites in NavMs identified by MD simulations. Alternating subunits are shown in dark/light blue. (B and D) Zoomed-in surface views of the extracellular (B) and S4-S5 linker binding sites (D). (C and E) The top six propofol binding poses at the extracellular binding site (C) and top 10 propofol binding poses at the S4-S5 linker binding site (E), from molecular docking simulations. (F) Time courses of the minimum distance between the bound propofol molecule and the residues lining the two binding sites, from MD simulations. For both sites, propofol binding occurred in three of the four subunits, denoted as Linker 1–3 and Extracellular 1–3; distances are not reported for the unoccupied subunit. Residues lining the S4-S5 linker site (left) consisted of V134, N212, and A221, and those lining the extracellular site (right) consisted of R186, M189, and K166.

modulate voltage sensor conformations of eukaryotic Navs (Sheets and Hanck, 2003, 2007; Muroi and Chanda, 2009), and (3) Na<sup>+</sup> channel blockers inhibit NavMs and hNav1.1 with comparable potencies and at similar binding sites (Bagnéris et al., 2014). It is conceivable that these similarities are determined by shared fundamental structural features that underlie slow inactivation in the pore domain as discussed above. Despite these observations, major structural features only found in eukaryotic Navs, such as their pseudotetrameric architecture and the III-IV cytoplasmic linker responsible for fast inactivation

(Vassilev et al., 1988; West et al., 1992; Catterall, 2012), could alter the ways in which anesthetics antagonize Nav function. These differences could explain why anesthetics do not stabilize the inactivated state of prokaryotic Navs (Fig. 2; Lee et al., 2012a,b; Barber et al., 2014; Sand et al., 2017) and why general anesthetics do not inhibit prokaryotic Navs by fast or slow open channel block (Fig. 3). Propofol might inhibit eukaryotic Navs through a combination of mechanisms that includes both the modulation of activation gating and slow inactivation that is conserved in prokaryotic Navs and local anesthetic-like mod-

ulation of fast inactivation gating with open pore block that is exclusive to eukaryotic Navs.

Ideally, quantitative global kinetic modeling examining multiple aspects of gating over a wide range of voltages would provide the most stringent test for possible mechanisms (Dougherty et al., 2008; Kaulin et al., 2008). This was unfortunately not experimentally feasible in this study because of limitations in patch stability, which prevented application of all voltage protocols to the same cell in the absence and presence of propofol. Nonetheless, we were able to produce robust datasets suitable for semiquantitative kinetic modeling, which served as a framework to formulate a plausible mechanism of action. These datasets yielded comprehensive experimental information on the various aspects of voltage-dependent gating (activation, deactivation, inactivation, and recovery from inactivation) over a wide range of voltages (−170 to +60 mV). Moreover, we performed these experiments at three relevant concentrations of propofol and repeated a critical subset of these experiments in both NaChBac and NavMs. Notably, the observed effects demonstrated little concentration dependence, which indicates that the concentrations of propofol tested may have been saturating. This is consistent with in vivo observations in tadpoles (Hall et al., 2010). We cannot, however, dismiss the possibility that cell-to-cell variability obscured concentration dependence, but in any case, the consistency of the results strengthens the conclusions.

## Conclusion

Mounting evidence points to voltage-gated Na<sup>+</sup> channels as important general anesthetic targets (Herold and Hemmings, 2012), but understanding the molecular mechanisms of this modulation is the first step toward identifying relevant anesthetic binding regions in Navs. We have found that propofol inhibits NaChBac and NavMs by promoting activation-coupled inactivation, which may involve multiple binding sites within the channel. Further investigation with mutational analysis will be required to assess the contributions of individual putative binding sites to the effects of propofol on these Navs. Moving forward, recent advances in photoaffinity labeling techniques and the availability of the full-length crystal structure for NavMs will permit in-depth structural investigations to help validate the significance of these sites in the mechanism of propofol action.

## Acknowledgments

We thank Tim Mosca for assistance rendering images.

This work was supported by the National Institute of General Medical Sciences of the National Institutes of Health awards P01GM55876 (to M. Covarrubias, V. Carnevale, and R. Eckenhoff) and F30GM123612 (to E. Yang).

The authors declare no competing financial interests.

Author contributions: E. Yang designed and conducted voltage-clamping experiments, analyzed and interpreted results, and wrote the manuscript. D. Granata conducted MD simulations and interpreted results. V. Carnevale designed and conducted MD simulations, analyzed and interpreted MD simulation results, and wrote the manuscript. R.G. Eckenhoff oversaw the study and pro-

vided critical feedback. M. Covarrubias oversaw study, designed experiments, interpreted results, and wrote the manuscript.

Kenton J. Swartz served as editor.

Submitted: 9 November 2017

Accepted: 12 June 2018

## References

- Ahern, C.A., J. Payandeh, F. Bosmans, and B. Chanda. 2016. The hitchhiker's guide to the voltage-gated sodium channel galaxy. *J. Gen. Physiol.* 147:1–24. <https://doi.org/10.1085/jgp.201511492>
- Aldrich, R.W., and C.F. Stevens. 1987. Voltage-dependent gating of single sodium channels from mammalian neuroblastoma cells. *J. Neurosci.* 7:418–431. <https://doi.org/10.1523/JNEUROSCI.07-02-00418.1987>
- Arcisio-Miranda, M., Y. Muroi, S. Chowdhury, and B. Chanda. 2010. Molecular mechanism of allosteric modification of voltage-dependent sodium channels by local anesthetics. *J. Gen. Physiol.* 136:541–554. <https://doi.org/10.1085/jgp.201010438>
- Armstrong, C.M. 1966. Time course of TEA(+)-induced anomalous rectification in squid giant axons. *J. Gen. Physiol.* 50:491–503. <https://doi.org/10.1085/jgp.50.2.491>
- Armstrong, C.M. 1971. Interaction of tetraethylammonium ion derivatives with the potassium channels of giant axons. *J. Gen. Physiol.* 58:413–437. <https://doi.org/10.1085/jgp.58.4.413>
- Armstrong, C.M. 1981. Sodium channels and gating currents. *Physiol. Rev.* 61:644–683. <https://doi.org/10.1152/physrev.1981.61.3.644>
- Armstrong, C.M. 2006. Na channel inactivation from open and closed states. *Proc. Natl. Acad. Sci. USA.* 103:17991–17996. <https://doi.org/10.1073/pnas.0607603103>
- Armstrong, C.M., and F. Bezanilla. 1977. Inactivation of the sodium channel. II. Gating current experiments. *J. Gen. Physiol.* 70:567–590. <https://doi.org/10.1085/jgp.70.5.567>
- Bagn  ris, C., P.G. DeCaen, C.E. Naylor, D.C. Pryde, I. Nobel, D.E. Clapham, and B.A. Wallace. 2014. Prokaryotic NavMs channel as a structural and functional model for eukaryotic sodium channel antagonism. *Proc. Natl. Acad. Sci. USA.* 111:8428–8433. <https://doi.org/10.1073/pnas.1406855111>
- Barber, A.F., Q. Liang, and M. Covarrubias. 2012. Novel activation of voltage-gated K(+) channels by sevoflurane. *J. Biol. Chem.* 287:40425–40432. <https://doi.org/10.1074/jbc.M112.405787>
- Barber, A.F., V. Carnevale, M.L. Klein, R.G. Eckenhoff, and M. Covarrubias. 2014. Modulation of a voltage-gated Na<sup>+</sup> channel by sevoflurane involves multiple sites and distinct mechanisms. *Proc. Natl. Acad. Sci. USA.* 111:6726–6731. <https://doi.org/10.1073/pnas.1405768111>
- Bean, B.P., C.J. Cohen, and R.W. Tsien. 1983. Lidocaine block of cardiac sodium channels. *J. Gen. Physiol.* 81:613–642. <https://doi.org/10.1085/jgp.81.5.613>
- Belelli, D., M. Pistis, J.A. Peters, and J.J. Lambert. 1999. General anaesthetic action at transmitter-gated inhibitory amino acid receptors. *Trends Pharmacol. Sci.* 20:496–502. [https://doi.org/10.1016/S0165-6147\(99\)01405-4](https://doi.org/10.1016/S0165-6147(99)01405-4)
- Bu, W., Q. Liang, L. Zhi, L. Maciunas, P.J. Loll, R.G. Eckenhoff, and M. Covarrubias. 2018. Sites and Functional Consequence of Alkylphenol Anesthetic Binding to Kv1.2 Channels. *Mol. Neurobiol.* 55:1692–1702. <https://doi.org/10.1007/s12035-017-0437-2>
- Buyan, A., D. Sun, and B. Corry. 2018. Protonation state of inhibitors determines interaction sites within voltage-gated sodium channels. *Proc. Natl. Acad. Sci. USA.* 115:E3135–E3144. <https://doi.org/10.1073/pnas.1714131115>
- Catterall, W.A. 2001. Physiology. A one-domain voltage-gated sodium channel in bacteria. *Science.* 294:2306–2308. <https://doi.org/10.1126/science.1067417>
- Catterall, W.A. 2012. Voltage-gated sodium channels at 60: structure, function and pathophysiology. *J. Physiol.* 590:2577–2589. <https://doi.org/10.1113/jphysiol.2011.224204>
- Catterall, W.A. 2015. Voltage-Gated Sodium Channels. J. Zheng, and M.C. Trudeau, editors. CRC Press, Taylor & Francis Group, Boca Raton, FL.
- Chiara, D.C., J.F. Gill, Q. Chen, T. Tillman, W.P. Dailey, R.G. Eckenhoff, Y. Xu, P. Tang, and J.B. Cohen. 2014. Photoaffinity labeling the propofol binding site in GLIC. *Biochemistry.* 53:135–142. <https://doi.org/10.1021/bi401492k>
- Covarrubias, M., A.F. Barber, V. Carnevale, W. Treptow, and R.G. Eckenhoff. 2015. Mechanistic Insights into the Modulation of Voltage-Gated Ion Channels by Inhalational Anesthetics. *Biophys. J.* 109:2003–2011. <https://doi.org/10.1016/j.bpj.2015.09.032>



- Dilger, J.P. 2002. The effects of general anaesthetics on ligand-gated ion channels. *Br. J. Anaesth.* 89:41–51. <https://doi.org/10.1093/bja/ae61>
- Dougherty, K., J.A. De Santiago-Castillo, and M. Covarrubias. 2008. Gating charge immobilization in Kv4.2 channels: The basis of closed-state inactivation. *J. Gen. Physiol.* 131:257–273. <https://doi.org/10.1085/jgp.200709938>
- Eger, E.I. II, L.J. Saidman, and B. Brandstater. 1965. Minimum alveolar anesthetic concentration: a standard of anesthetic potency. *Anesthesiology*. 26:756–763. <https://doi.org/10.1097/00005542-196511000-00010>
- Feng, A.Y., A.D. Kaye, R.J. Kaye, K. Belani, and R.D. Urman. 2017. Novel propofol derivatives and implications for anesthesia practice. *J. Anaesthesiol. Clin. Pharmacol.* 33:9–15. <https://doi.org/10.4103/0970-9185.202205>
- Fineberg, J.D., D.M. Ritter, and M. Covarrubias. 2012. Modeling-independent elucidation of inactivation pathways in recombinant and native A-type Kv channels. *J. Gen. Physiol.* 140:513–527. <https://doi.org/10.1085/jgp.201210869>
- Finol-Urdaneta, R.K., Y. Wang, A. Al-Sabi, C. Zhao, S.Y. Noskov, and R.J. French. 2014. Sodium channel selectivity and conduction: Prokaryotes have devised their own molecular strategy. *J. Gen. Physiol.* 143:157–171. <https://doi.org/10.1085/jgp.201311037>
- Franks, N.P. 2008. General anaesthesia: from molecular targets to neuronal pathways of sleep and arousal. *Nat. Rev. Neurosci.* 9:370–386. <https://doi.org/10.1038/nrn2372>
- Friesner, R.A., Murphy, R.B., Repasky, M. P., Frye, L. L., Greenwood, J. R., Halgren, T. A., Sanschargin, P.C., Mainz, D. T. (2006). Extra Precision Glide: Docking and Scoring Incorporating a Model of Hydrophobic Enclosure for Protein–Ligand Complexes. doi: <https://doi.org/10.1021/JM051256O>
- Goldschen-Ohm, M.P., and B. Chanda. 2014. Probing gating mechanisms of sodium channels using pore blockers. In *Voltage Gated Sodium Channels*. Vol. 221. P.C. Ruben, editor. Springer, Heidelberg. 183–201.
- Haeseler, G., M. Störmer, J. Bufler, R. Dengler, H. Hecker, S. Piepenbrock, and M. Leuwer. 2001. Propofol blocks human skeletal muscle sodium channels in a voltage-dependent manner. *Anesth. Analg.* 92:1192–1198. <https://doi.org/10.1097/00005539-200105000-00021>
- Hales, T.G., and J.J. Lambert. 1991. The actions of propofol on inhibitory amino acid receptors of bovine adrenomedullary chromaffin cells and rodent central neurones. *Br. J. Pharmacol.* 104:619–628. <https://doi.org/10.1111/j.1476-5381.1991.tb12479.x>
- Hall, M.A., J. Xi, C. Lor, S. Dai, R. Pearce, W.P. Dailey, and R.G. Eckenhoff. 2010. m-Azipropofol (AziPm) a photoactive analogue of the intravenous general anesthetic propofol. *J. Med. Chem.* 53:5667–5675. <https://doi.org/10.1021/jm1004072>
- Harder, E., W. Damm, J. Maple, C. Wu, M. Reboul, J.Y. Xiang, L. Wang, D. Lupyán, M.K. Dahlgren, J.L. Knight, et al. 2016. OPLS3: A Force Field Providing Broad Coverage of Drug-like Small Molecules and Proteins. *J. Chem. Theory Comput.* 12:281–296. <https://doi.org/10.1021/acs.jctc.5b00864>
- Hemmings, H.C. Jr., M.H. Akabas, P.A. Goldstein, J.R. Trudell, B.A. Orser, and N.L. Harrison. 2005. Emerging molecular mechanisms of general anesthetic action. *Trends Pharmacol. Sci.* 26:503–510. <https://doi.org/10.1016/j.tips.2005.08.006>
- Herold, K.F., and H.C. Hemmings Jr. 2012. Sodium channels as targets for volatile anesthetics. *Front. Pharmacol.* 3:50. <https://doi.org/10.3389/fphar.2012.00050>
- Hille, B. 1977. Local anesthetics: Hydrophilic and hydrophobic pathways for the drug-receptor reaction. *J. Gen. Physiol.* 69:497–515. <https://doi.org/10.1085/jgp.69.4.497>
- James, R., and J.B. Glen. 1980. Synthesis, biological evaluation, and preliminary structure-activity considerations of a series of alkylphenols as intravenous anesthetic agents. *J. Med. Chem.* 23:1350–1357. <https://doi.org/10.1021/jm00186a013>
- Jayakar, S.S., W.P. Dailey, R.G. Eckenhoff, and J.B. Cohen. 2013. Identification of propofol binding sites in a nicotinic acetylcholine receptor with a photoreactive propofol analog. *J. Biol. Chem.* 288:6178–6189. <https://doi.org/10.1074/jbc.M112.435909>
- Jayakar, S.S., X. Zhou, D.C. Chiara, Z. Dostalova, P.Y. Savechenkov, K.S. Bruzik, W.P. Dailey, K.W. Miller, R.G. Eckenhoff, and J.B. Cohen. 2014. Multiple propofol-binding sites in a  $\gamma$ -aminobutyric acid type A receptor (GABA<sub>A</sub>R) identified using a photoreactive propofol analog. *J. Biol. Chem.* 289:27456–27468. <https://doi.org/10.1074/jbc.M114.581728>
- Jorgensen, W.L., D.S. Maxwell, and J. Tirado-Rives. 1996. Development and testing of the OPLS all-atom force field on conformational energetics and properties of organic liquids. *J. Am. Chem. Soc.* 118:11225–11236. <https://doi.org/10.1021/ja9621760>
- Jurd, R., M. Arras, S. Lambert, B. Drexler, R. Siegwart, F. Crestani, M. Zaugg, K.E. Vogt, B. Ledermann, B. Antkowiak, et al. 2003. General anesthetic actions in vivo strongly attenuated by a point mutation in the GABA(A) receptor beta3 subunit. *FASEB J.* 17:250–252. <https://doi.org/10.1096/fj.02-0611fje>
- Kaulin, Y.A., J.A. De Santiago-Castillo, C.A. Rocha, and M. Covarrubias. 2008. Mechanism of the modulation of Kv4:KChIP-1 channels by external K<sup>+</sup>. *Biophys. J.* 94:1241–1251. <https://doi.org/10.1529/biophysj.107.117796>
- Kinde, M.N., V. Bondarenko, D. Granata, W. Bu, K.C. Grasty, P.J. Loll, V. Carnevale, M.L. Klein, R.G. Eckenhoff, P. Tang, and Y. Xu. 2016. Fluorine-19 NMR and computational quantification of isoflurane binding to the voltage-gated sodium channel NaChBac. *Proc. Natl. Acad. Sci. USA.* 113:13762–13767. <https://doi.org/10.1073/pnas.1609939113>
- Kuo, C.C., and B.P. Bean. 1994. Na<sup>+</sup> channels must deactivate to recover from inactivation. *Neuron.* 12:819–829. [https://doi.org/10.1016/0896-6273\(94\)90335-2](https://doi.org/10.1016/0896-6273(94)90335-2)
- Kuzmenkin, A., F. Bezanilla, and A.M. Correa. 2004. Gating of the bacterial sodium channel, NaChBac: Voltage-dependent charge movement and gating currents. *J. Gen. Physiol.* 124:349–356. <https://doi.org/10.1085/jgp.200409139>
- LeBard, D.N., J. Hénin, R.G. Eckenhoff, M.L. Klein, and G. Brannigan. 2012. General anesthetics predicted to block the GLIC pore with micromolar affinity. *PLOS Comput. Biol.* 8:e1002532. <https://doi.org/10.1371/journal.pcbi.1002532>
- Lee, S., S.J. Goodchild, and C.A. Ahern. 2012a. Local anesthetic inhibition of a bacterial sodium channel. *J. Gen. Physiol.* 139:507–516. <https://doi.org/10.1085/jgp.201210779>
- Lee, S., S.J. Goodchild, and C.A. Ahern. 2012b. Molecular and functional determinants of local anesthetic inhibition of NaChBac. *Channels (Austin)*. 6:403–406. <https://doi.org/10.4161/chan.21807>
- Lee, S., A. Tran, M. Allsopp, J.B. Lim, J. Hénin, and J.B. Klauda. 2014. CHA RMM36 united atom chain model for lipids and surfactants. *J. Phys. Chem. B.* 118:547–556. <https://doi.org/10.1021/jp410344g>
- Li, X., K. Pan, D. Zhu, Y. Li, and G. Tao. 2016. Propofol postsynaptically suppresses stellate neuron excitability in the entorhinal cortex by influencing the HCN and TREK-2 channels. *Neurosci. Lett.* 619:54–59. <https://doi.org/10.1016/j.neulet.2016.03.014>
- Liang, Q., W.D. Anderson, S.T. Jones, C.S. Souza, J.M. Hosoume, W. Treptow, and M. Covarrubias. 2015. Positive Allosteric Modulation of Kv Channels by Sevoflurane: Insights into the Structural Basis of Inhaled Anesthetic Action. *PLoS One.* 10:e0143363. <https://doi.org/10.1371/journal.pone.0143363>
- Lin, L.H., L.L. Chen, J.A. Zirrollo, and R.A. Harris. 1992. General anesthetics potentiate gamma-aminobutyric acid actions on gamma-aminobutyric acidA receptors expressed by *Xenopus* oocytes: lack of involvement of intracellular calcium. *J. Pharmacol. Exp. Ther.* 263:569–578.
- Long, S.B., E.B. Campbell, and R. MacKinnon. 2005. Voltage Sensor of Kv1.2: Structural Basis of Electromechanical Coupling. *Science.* 309:903–908. <https://doi.org/10.1126/science.1105528>
- McCusker, E.C., C. Bagnéris, C.E. Naylor, A.R. Cole, N. D’Avanzo, C.G. Nichols, and B.A. Wallace. 2012. Structure of a bacterial voltage-gated sodium channel pore reveals mechanisms of opening and closing. *Nat. Commun.* 3:1102. <https://doi.org/10.1038/ncomms2077>
- Muroi, Y., and B. Chanda. 2009. Local anesthetics disrupt energetic coupling between the voltage-sensing segments of a sodium channel. *J. Gen. Physiol.* 133:1–15. <https://doi.org/10.1085/jgp.200810103>
- Naylor, C.E., C. Bagnéris, P.G. DeCaen, A. Sula, A. Scaglione, D.E. Clapham, and B.A. Wallace. 2016. Molecular basis of ion permeability in a voltage-gated sodium channel. *EMBO J.* 35:820–830. <https://doi.org/10.15252/emboj.201593285>
- Nurani, G., M. Radford, K. Charalambous, A.O. O’Reilly, N.B. Cronin, S. Haque, and B.A. Wallace. 2008. Tetrameric bacterial sodium channels: characterization of structure, stability, and drug binding. *Biochemistry.* 47:8114–8121. <https://doi.org/10.1021/bi800645w>
- Nury, H., C. Van Renterghem, Y. Weng, A. Tran, M. Baaden, V. Dufresne, J.P. Changeux, J.M. Sonner, M. Delarue, and P.J. Corringer. 2011. X-ray structures of general anaesthetics bound to a pentameric ligand-gated ion channel. *Nature.* 469:428–431. <https://doi.org/10.1038/nature09647>
- Orser, B.A., L.Y. Wang, P.S. Pennefather, and J.F. MacDonald. 1994. Propofol modulates activation and desensitization of GABA<sub>A</sub> receptors in cultured murine hippocampal neurons. *J. Neurosci.* 14:7747–7760. <https://doi.org/10.1523/JNEUROSCI.14-12-07747.1994>
- OuYang, W., and H.C. Hemmings Jr. 2007. Isoform-selective effects of isoflurane on voltage-gated Na<sup>+</sup> channels. *Anesthesiology.* 107:91–98. <https://doi.org/10.1097/01.anes.0000268390.28362.4a>



- Ouyang, W., G. Wang, and H.C. Hemmings Jr. 2003. Isoflurane and propofol inhibit voltage-gated sodium channels in isolated rat neurohypophyseal nerve terminals. *Mol. Pharmacol.* 64:373–381. <https://doi.org/10.1124/mol.64.2.373>
- Ouyang, W., T.-Y. Jih, T.-T. Zhang, A.M. Correa, and H.C. Hemmings Jr. 2007. Isoflurane inhibits NaChBac, a prokaryotic voltage-gated sodium channel. *J. Pharmacol. Exp. Ther.* 322:1076–1083. <https://doi.org/10.1124/jpet.107.122929>
- Ouyang, W., K.F. Herold, and H.C. Hemmings Jr. 2009. Comparative effects of halogenated inhaled anesthetics on voltage-gated Na<sup>+</sup> channel function. *Anesthesiology*. 110:582–590. <https://doi.org/10.1097/ALN.0b013e318197941e>
- Pavlov, E., C. Bladen, R. Winkfein, C. Diao, P. Dhaliwal, and R.J. French. 2005. The pore, not cytoplasmic domains, underlies inactivation in a prokaryotic sodium channel. *Biophys. J.* 89:232–242. <https://doi.org/10.1529/biophysj.104.056994>
- Payandeh, J., T. Scheuer, N. Zheng, and W.A. Catterall. 2011. The crystal structure of a voltage-gated sodium channel. *Nature*. 475:353–358. <https://doi.org/10.1038/nature10238>
- Phillips, J.C., R. Braun, W. Wang, J. Gumbart, E. Tajkhorshid, E. Villa, C. Chipot, R.D. Skeel, L. Kalé, and K. Schulten. 2005. Scalable molecular dynamics with NAMD. *J. Comput. Chem.* 26:1781–1802. <https://doi.org/10.1002/jcc.20289>
- Raju, S.G., A.F. Barber, D.N. LeBard, M.L. Klein, and V. Carnevale. 2013. Exploring volatile general anesthetic binding to a closed membrane-bound bacterial voltage-gated sodium channel via computation. *PLOS Comput. Biol.* 9:e1003090. <https://doi.org/10.1371/journal.pcbi.1003090>
- Rehberg, B., and D.S. Duch. 1999. Suppression of central nervous system sodium channels by propofol. *Anesthesiology*. 91:512–520. <https://doi.org/10.1097/00000542-199908000-00026>
- Ren, D., B. Navarro, H. Xu, L. Yue, Q. Shi, and D.E. Clapham. 2001. A prokaryotic voltage-gated sodium channel. *Science*. 294:2372–2375. <https://doi.org/10.1126/science.1065635>
- Sand, R.M., K.J. Gingrich, T. Macharadze, K.F. Herold, and H.C. Hemmings Jr. 2017. Isoflurane modulates activation and inactivation gating of the prokaryotic Na<sup>+</sup> channel NaChBac. *J. Gen. Physiol.* 149:623–638. <https://doi.org/10.1085/jgp.201611600>
- Santiago-Castillo, J.A., M. Covarrubias, J.E. Sánchez-Rodríguez, P. Perez-Cornejo, and J. Arreola. 2010. Simulating complex ion channel kinetics with IonChannelLab. *Channels (Austin)*. 4:422–428. <https://doi.org/10.4161/chan.4.5.13404>
- Sastry, G.M., M. Adzhigirey, T. Day, R. Annabhimoju, and W. Sherman. 2013. Protein and ligand preparation: parameters, protocols, and influence on virtual screening enrichments. *J. Comput. Aided Mol. Des.* 27:221–234. <https://doi.org/10.1007/s10822-013-9644-8>
- Sheets, M.F., and D.A. Hanck. 2003. Molecular action of lidocaine on the voltage sensors of sodium channels. *J. Gen. Physiol.* 121:163–175. <https://doi.org/10.1085/jgp.20028651>
- Sheets, M.F., and D.A. Hanck. 2007. Outward stabilization of the S4 segments in domains III and IV enhances lidocaine block of sodium channels. *J. Physiol.* 582:317–334. <https://doi.org/10.1113/jphysiol.2007.134262>
- Shin, K.S., B.S. Rothberg, and G. Yellen. 2001. Blocker state dependence and trapping in hyperpolarization-activated cation channels: Evidence for an intracellular activation gate. *J. Gen. Physiol.* 117:91–101. <https://doi.org/10.1085/jgp.117.2.91>
- Stoetzer, C., S. Reuter, T. Doll, N. Foadi, F. Wegner, and A. Leffler. 2016. Inhibition of the cardiac Na<sup>+</sup> channel  $\alpha$ -subunit Nav1.5 by propofol and dexmedetomidine. *Naunyn-Schmiedeberg's Arch. Pharmacol.* 389:315–325. <https://doi.org/10.1007/s00210-015-1195-1>
- Strichartz, G.R. 1973. The inhibition of sodium currents in myelinated nerve by quaternary derivatives of lidocaine. *J. Gen. Physiol.* 62:37–57. <https://doi.org/10.1085/jgp.62.1.37>
- Sula, A., J. Booker, L.C.T. Ng, C.E. Naylor, P.G. DeCaen, and B.A. Wallace. 2017. The complete structure of an activated open sodium channel. *Nat. Commun.* 8:14205. <https://doi.org/10.1038/ncomms14205>
- Tilegenova, C., D.M. Cortes, and L.G. Cuello. 2017. Hysteresis of KcsA potassium channel's activation-deactivation gating is caused by structural changes at the channel's selectivity filter. *Proc. Natl. Acad. Sci. USA*. 114:3234–3239. <https://doi.org/10.1073/pnas.1618101114>
- Ton, H.T., T.X. Phan, A.M. Abramyan, L. Shi, and G.P. Ahern. 2017. Identification of a putative binding site critical for general anesthetic activation of TRPA1. *Proc. Natl. Acad. Sci. USA*. 114:3762–3767. <https://doi.org/10.1073/pnas.1618144114>
- Ulmschneider, M.B., C. Bagnéris, E.C. McCusker, P.G. DeCaen, M. Delling, D.E. Clapham, J.P. Ulmschneider, and B.A. Wallace. 2013. Molecular dynamics of ion transport through the open conformation of a bacterial voltage-gated sodium channel. *Proc. Natl. Acad. Sci. USA*. 110:6364–6369. <https://doi.org/10.1073/pnas.1214667110>
- Vassilev, P.M., T. Scheuer, and W.A. Catterall. 1988. Identification of an intracellular peptide segment involved in sodium channel inactivation. *Science*. 241:1658–1661. <https://doi.org/10.1126/science.2458625>
- Wang, Y., et al. 2018. Propofol inhibits the voltage-gated sodium channel NaChBac at multiple sites. *J. Gen. Physiol.* <https://doi.org/10.1085/jgp.201811993>
- Wang, S.-Y., J. Mitchell, E. Moczydlowski, and G.K. Wang. 2004. Block of inactivation-deficient Na<sup>+</sup> channels by local anesthetics in stably transfected mammalian cells: Evidence for drug binding along the activation pathway. *J. Gen. Physiol.* 124:691–701. <https://doi.org/10.1085/jgp.200409128>
- Weng, Y., L. Yang, P.-J. Corringer, and J.M. Sonner. 2010. Anesthetic sensitivity of the Gloeobacter violaceus proton-gated ion channel. *Anesth. Analg.* 110:59–63. <https://doi.org/10.1213/ANE.0b013e3181c4bc69>
- West, J.W., D.E. Patton, T. Scheuer, Y. Wang, A.L. Goldin, and W.A. Catterall. 1992. A cluster of hydrophobic amino acid residues required for fast Na<sup>+</sup>-channel inactivation. *Proc. Natl. Acad. Sci. USA*. 89:10910–10914. <https://doi.org/10.1073/pnas.89.22.10910>
- Woll, K.A., W. Peng, Q. Liang, L. Zhi, J.A. Jacobs, L. Maciunas, N. Bhanu, B.A. Garcia, M. Covarrubias, P.J. Loll, et al. 2017a. Photoaffinity Ligand for the Inhalational Anesthetic Sevoflurane Allows Mechanistic Insight into Potassium Channel Modulation. *ACS Chem. Biol.* 12:1353–1362. <https://doi.org/10.1021/acscchembio.7b00222>
- Woll, K.A., K.A. Skinner, E. Gianti, N.V. Bhanu, B.A. Garcia, V. Carnevale, R.G. Eckenhoff, and R. Gaudet. 2017b. Sites Contributing to TRPA1 Activation by the Anesthetic Propofol Identified by Photoaffinity Labeling. *Biophys. J.* 113:2168–2172. <https://doi.org/10.1016/j.bpj.2017.08.040>
- Woll, K.A., B.P. Weiser, Q. Liang, T. Meng, A. McKinstry-Wu, B. Pinch, W.P. Dailey, W.D. Gao, M. Covarrubias, and R.G. Eckenhoff. 2015. Role for the propofol hydroxyl in anesthetic protein target molecular recognition. *ACS Chem. Neurosci.* 6:927–935. <https://doi.org/10.1021/acscchemneuro.5b00078>
- Woll, K.A., X. Zhou, N.V. Bhanu, B.A. Garcia, M. Covarrubias, K.W. Miller, and R.G. Eckenhoff. 2018. Identification of binding sites contributing to volatile anesthetic effects on GABA type A receptors. *FASEB J.* fj201701347R. <https://doi.org/10.1096/fj.201701347R>
- Xiong, W., R.A. Li, Y. Tian, and G.F. Tomaselli. 2003. Molecular motions of the outer ring of charge of the sodium channel: Do they couple to slow inactivation? *J. Gen. Physiol.* 122:323–332. <https://doi.org/10.1085/jgp.200308881>
- Yan, Z., Q. Zhou, L. Wang, J. Wu, Y. Zhao, G. Huang, W. Peng, H. Shen, J. Lei, and N. Yan. 2017. Structure of the Na<sub>v</sub>1.4- $\beta$ 1 Complex from Electric Eel. *Cell*. 170:470–482.e11. <https://doi.org/10.1016/j.cell.2017.06.039>
- Zecharia, A.Y., L.E. Nelson, T.C. Gent, M. Schumacher, R. Jurd, U. Rudolph, S.G. Brickley, M. Maze, and N.P. Franks. 2009. The involvement of hypothalamic sleep pathways in general anesthesia: testing the hypothesis using the GABAA receptor  $\beta$ 3N265M knock-in mouse. *J. Neurosci.* 29:2177–2187. <https://doi.org/10.1523/JNEUROSCI.4997-08.2009>
- Zhang, J., X. Qu, M. Covarrubias, and M.W. Germann. 2013. Insight into the modulation of Shaw2 Kv channels by general anesthetics: Structural and functional studies of S4-S5 linker and S6 C-terminal peptides in micelles by NMR. *Biochim. Biophys. Acta*. 1828:595–601. <https://doi.org/10.1016/j.bbame.2012.09.025>
- Zhang, X., W. Ren, P. DeCaen, C. Yan, X. Tao, L. Tang, J. Wang, K. Hasegawa, T. Kumasaka, J. He, et al. 2012. Crystal structure of an orthologue of the NaChBac voltage-gated sodium channel. *Nature*. 486:130–134. <https://doi.org/10.1038/nature11054>
- Zhou, C., J. Liu, and X.-D. Chen. 2012. General anesthesia mediated by effects on ion channels. *World J. Crit. Care Med.* 1:80–93. <https://doi.org/10.5492/wjccm.v1.i3.80>